

CHAPTER I

INTRODUCTION

The Advanced Photon Source (APS) is a national synchrotron-radiation light source research facility generating high brilliance X-ray beams. The APS storage ring operation at a higher beam current is one of the potential enhancements to increase beam brilliance [21]*. Currently, the 7GeV APS storage ring operates at 100mA.

Operation at higher beam currents would impact the requirements of several beam line components, accelerator hardware, optics, front ends, and crotch absorbers. The absorbers at APS are water cooled and made out of Glidcop Al-15 (Alumina dispersion strengthened copper) [6] with high tensile and fatigue strengths at elevated temperatures and high thermal conductivity. One of the probable enhancements to the absorbers would be to increase heat transfer. To increase the heat transfer there is a need to increase the velocity of the cooling water. But, there is a need to predict the amount and the rate of erosion that takes place at higher water velocities. A study of the erosion of Glidcop tubing was carried out with water circulating for approximately six months at different velocities 15ft/s, 20ft/s, 25ft/s and 30ft/s. A finite element analysis of the absorbers at APS was conducted to better understand the temperature distribution and the peak temperatures achievable with a variable heat flux distribution applied due to the X-ray beam impact. A 3-D model of the absorber was created using ANSYS 7.1.

* Corresponds to numbered references in the bibliography

CHAPTER II

LITERATURE REVIEW

2.1 Introduction of the Mechanism of X-ray Beam Production at the APS

The APS is a third-generation X-ray source, which produces high brilliance X-ray beams. The X-ray beams are used in scientific and medical fields for research. X-rays are produced with the help of a series of 5 major components: a linear accelerator (Linac), accumulator ring, booster/synchrotron, storage ring and beam lines [21] as shown in Figure 2.1.

The beam acceleration and the storage process begin at the electron gun in the linear accelerator (LINAC), which emits electrons that exit the gun at 100KeV. The energy is then raised to 450MeV by a series of accelerating structures.

The APS positron accumulator ring (PAR) is a 450MeV ring that accumulates electrons from the linear accelerator for injection into the synchrotron (booster). The electron beam energy is raised to 7 GeV in the booster using electrical field supplied by radio frequency (rf) cavities. From the booster the electrons are then injected into the storage ring, which has a circumference of 1104m and is located inside the experimental hall. The storage ring has 40 sectors-5 sectors are equipped with injection and rf equipment and 35 are equipped to provide insertion devices and bending magnet radiation. Each of the 35 sectors has two beams: one originating at a bending magnet in

the storage ring lattice and the other at an insertion device. The beam of electrons is steered and focused by 1097 powerful electromagnets. The beam decelerates at a rate of about 6MeV per turn as it emits synchrotron radiation. This energy loss is replaced by the 352MHz storage ring rf system. Third generation storage rings maximize the X-ray beam qualities- flux and brilliance. Bending magnets and insertion devices are major components for the production of X-rays. When a charged particle is accelerated, so that either its speed or trajectory is changed, radiation will be emitted.

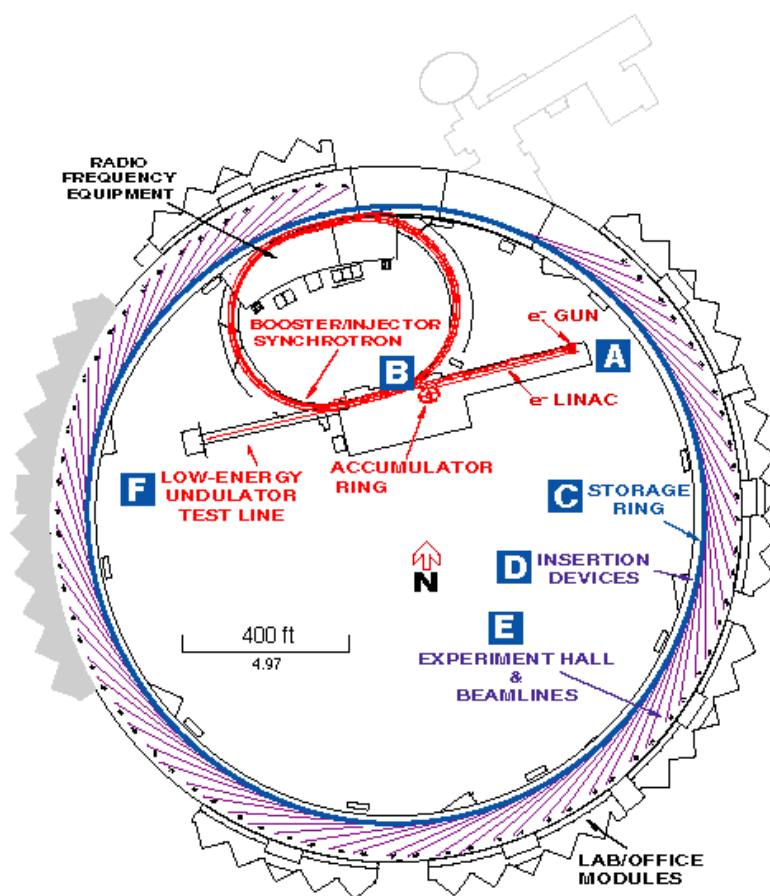


Figure 2.1. The Advanced Photon Source X-ray Production Facility

As the electrons in the beam are accelerated, the bending magnets, making the beams go in a curved path, alter their trajectory. At each of these bends, X-rays are emitted which go off in a tangential direction to the arc of the particle beam.

The insertion devices are composed mainly of the undulators. The insertion devices are the N-S permanent magnets with alternating polarities placed in the path of the beam. When spaced together, the undulators have lower fields, and have a narrow cone of radiation. The APS insertion devices deliver high-brilliance beams in the X-ray region from 2.5KeV to 100KeV. The APS insertion device design is flexible and versatile, meaning different devices can operate simultaneously at different locations around the storage ring.

The X-ray beam thus produced is absorbed at various places; only a portion of the width is used for scientific research while absorbers and collimators intercept the rest. The present storage ring current is 100mA. Future plans are to raise this current to 300mA. Detailed analysis is underway in this regard. The small portion of the X-ray fan that is used is concentrated in medical, biological and many other scientific research areas.

2.2 Glidcop

2.2.1 Introduction: Dispersion strengthened copper is known by the trade name Glidcop [15]. Glidcop is a high performance copper material. It sustains high heat loads and flux. It has almost the same thermal and electrical conductivities as copper but it

manifests superior mechanical properties. It possesses high yield strength of greater than 60,000psi, and it has high fatigue resistance under cyclic loads. It does not anneal at brazing temperatures, but it cannot be electron-beam welded and is difficult to braze [16].

In a design where high electrical conductivity and mechanical strength are required, the use of Glidcop precludes having to fabricate the component out of a high strength material such as stainless steel and applying copper plating afterwards. Glidcop can be applied to design with just about the same considerations as OFE copper relative to machinability and joinability [6].

The Glidcop AL-15 is primarily designed for applications requiring the highest electrical and thermal conductivities along with good elevated temperature strength. It has excellent cold-working characteristics, and can be drawn into fine wire or rolled into thin sheets. Glidcop affords the designer new opportunities to optimize designs that are exposed to high temperature in processing or in use. Glidcop can sustain operational heat flux levels up to $30\text{W}/\text{mm}^2$. The compositions of three commonly used grades of Glidcop are provided in Table 2.1 [6].

Table 2.1. Types of Glidcop and Their Composition

Grade	Component	Weight%
Glidcop Al-15	Al ₂ O ₃	0.3
	Cu	99.7
Glidcop Al -25	Al ₂ O ₃	0.5
	Cu	99.5
Glidcop Al -60	Al ₂ O ₃	1.1
	Cu	98.9

2.2.2 Material Notes: Glidcop is copper that is dispersion strengthened with a very small percentage of ultra fine particles of aluminum oxide. It is produced using an internal oxidation powder metallurgy process whereby aluminum oxide is formed in the Cu matrix. The matrix is hardened while the copper electrical and thermal conductivities are minimally lowered. The aluminum oxide particles are very thermally stable and remain effective in strengthening the copper matrix and resisting grain coarsening, even after very long exposures to high temperatures during brazing or high temperature duty cycles.

Glidcop is available in three different levels of Al₂O₃. Increasing the Al₂O₃ levels will increase strength but decrease conductivities. All three grades can be further strengthened by cold work. Glidcop is available in a wide range of extruded and drawn shapes and sizes, including rounds, rectangles, wires, plates, tubes, and strip due to this material structure. It is also available in a limited proportion in the powder form. All the

different types of Glidcop along with their associated properties are given in Table 2.2[17, 14].

Table 2.2. Types of Glidcop and Their Properties

	Al -15	Al -25	Al -60
Mechanical Properties			
Tensile Strength, Yield (MPa)	255-300	296-372	413-517
Electrical Properties			
Electrical Resistivity (ohm-cm)	1.85×10^{-6}	2.0×10^{-6}	2.2×10^{-6}
Thermal Properties			
Thermal Conductivity (W/m-k)	365	344	322

2.2.3 Applications: At the APS many of the high heat load components use Glidcop as the base material. Components being hermetically sealed in glass, soldered or brazed can be optimized with Glidcop. Glidcop is recommended for hybrid circuit package components, vacuum tube, microwave tube and cathodes, helices and heat sinks and electrical components such as circuit breakers. It is also used in relay blades and switches, rotating equipment components such as commutators, electric generator and motor components, brush springs, and high power magnet windings.

Low Oxygen (LOX) Glidcop is used for applications requiring brazed joints and/or extended high temperature exposure in hydrogen under pressure or in vacuum. Glidcop Al-60 is used for applications that require greater strength at the expense of lower electrical conductivity. Glidcop Al-15 is a new alumina content grade of

dispersion-strengthened copper. It consists of a pure copper matrix containing finely dispersed strengthened sub-microscopic particles of aluminum oxide. This alloy is now available in a low oxygen version, which can be exposed to hydrogen at high temperature without embrittlement. This material has very high electrical and thermal conductivities and also high strength after exposure to elevated temperatures. Glidcop Al-15 is available in many forms including rod and bar, strip, wire, and wire redraw.

Glidcop has been successfully applied to accelerator designs primarily for two reasons. First, it has comparable electrical and thermal properties to OFE copper and can be substituted for OFE in areas where high strength and high conductivity are required. Second, it can be fabricated into shapes and assemblies using processes that are very similar to those used with OFE copper. Reliable high temperature data enables the accurate prediction of the response of Glidcop at very elevated temperatures where the strength has diminished to approximately 1% of the room temperature strength [12]. Information about the fracture toughness properties of Glidcop can be obtained from [19].

2.2.4 Erosion Corrosion Characteristics: Erosion corrosion is the wear and corrosion caused by a rapidly flowing liquid. The extent of the attack depends on the degree of turbulence. Pits formed by erosion corrosion usually have bright surfaces free from corrosion products. They often have a characteristic horseshoe shape with the flanks pointing in the direction of flow and in the cross-section; the pits are usually undercut in the direction of flow.

Erosion corrosion may occur in water pipes when the flow velocity is high, particularly when the flow is disturbed, e.g., at unsuitably formed branches, connections or bends. Attack sometimes occurs in straight tubes, usually in the form of streaks along the tube. Erosion corrosion is also promoted by gas bubbles and by solid particles suspended in permissible flow velocity of 1.5m/s at continuous flow, which is actually recommended. There is no recommendation for water of intermittent flow.

Normally, a thin film of cuprous and cupric oxide forms on exposed copper surfaces. This film provides protection of the metal surface from wear. However, the formation of this protective layer can be hindered by high flow velocities and, thus, the removal of the material may be accelerated due to mechanical and chemical action. When material loss occurs caused by localized attack, due to curvature within the flow system, it is referred to as impingement [7]. The extent of the inroad depends upon a number of factors. Among these factors are turbulence, chemical composition, velocity, temperature, and, of course, time. Although limited in quantity, past experimentation offers some generalizations about the influence of these parameters on the erosion corrosion of copper [8]. In this section the erosion corrosion properties of copper and Glidcop are discussed from the technical papers collected in these areas.

In certain fusion energy applications, high velocity, sub-cooled water must be provided to cool high heat flux components. Because of its high heat transfer properties, copper turns out to be an attractive material to use for the coolant tube walls. The existing

literature shows evidence of erosion corrosion in copper and Glidcop at above 7 m/s. In general, the erosion corrosion occurred to a greater extent in copper rather than Glidcop [10].

One case of interest is a large superconducting tokamak [1] with long pulse (30 second) operation. The tokamak has been designed and is currently being constructed in France. It will require a pump limiter system and will allow control of the plasma density and particle recycling. The leading edge adjacent to the particle collection throat will receive a large heat flux of approximately 3-4 kW/cm². In order to cool this area, high velocity sub-cooled water is necessary. The water velocity will be as high as 11-13 m/s. Unfortunately, high water velocities may lead to erosion corrosion [2] of the coolant tube inner wall and perhaps, eventually to perforation.

There is little existing literature which predicts the effects of flow velocities as high as those demanded by the above system. Oak Ridge National Laboratory performed the most extensive experimentation under plasma conditions with copper swirl tubes. They did not observe failure after 25,000 full power pulses for a cumulative 100,000 beam seconds [3]. However, no actual information on the extent of the erosion corrosion was obtainable. A separate study, of the effect of water flowing at approximately 12m/s was performed in Sandia Laboratories [25]. In order to satisfy thermal conductivity requirements, and because of its known resistance to erosion corrosion, copper and an alloy of copper (Glidcop Al-15) were drawn into tubing and employed in the experiment [4,5].

The experiments at Sandia were conducted by inserting the two tube specimens, one copper and the other Glidcop, into a closed loop flow system. Water flowing at approximately 4ft/s was circulated for approximately 582 hours. After the experiment, inspections were mainly carried out at the bends, as erosion corrosion is more likely to occur in regions of high curvature.

The initial inspection revealed that bands or striations of black color had formed in the Glidcop bends but not in the copper. When the tubes were cut and examined under magnification, it was found that the copper tubing actually had experienced erosion corrosion to a greater extent than the Glidcop tubing, in spite of the observed striations. The Glidcop showed evidence of a slightly different form of corrosion onslaught, pitting [10]. Pitting is a form of centralized corrosion, which results in small regions of deep penetrating attack. There was no significant difference between the wall thickness measurements before or after the experiment for either the copper or the Glidcop tubing. A surface heat flux could be an important factor in this erosion corrosion process, because it could cause surface boiling at the inner tube wall. This would be deleterious since the cavitation of the bubbles would destroy or prevent the formation of protective films that would form on the copper surface. Also, the boiling would add a synergistic element to the impingement attack caused by the flowing water. Thus copper and Glidcop could exhibit more erosion corrosion under similar flow conditions in the presence of a surface heat flux [11]. It was concluded in [18] that Glidcop would perform better than copper under these circumstances.

From the past experiments cited above, it can be concluded that the following factors have to be controlled during erosion experiments.

- Flow velocity
- Water temperature
- Water composition
- pH value of water
- Oxygen content in water
- Flow duration
- Tube diameter
- Hardness of the material
- Installation conditions

The results found from earlier work can be summarized as follows:

- For aerated water with moderate corrosivity (pH 8) and continuous flow, the maximum flow velocity not causing erosion corrosion was 3m/s at 65 °C and 6m/s at 30 °C in small (6/4mm) diameter tubes.
- With intermittent flow (<25% of the time) of the same water (pH 8) no erosion corrosion was caused in 6/4mm diameter tubes at either temperature with a flow velocity as high as 12m/s.
- For the more corrosive aerated water (pH 6.5), with continuous flow, the velocity must be maintained at a lower level; e.g., at 65 °C attack was found when the velocity was >1m/s.

- For water low in oxygen (de-aerated water), e.g., in central heating systems, higher flow velocities are acceptable; thus 12m/s did not cause attack in small (6/4mm) diameter tubes with the moderately corrosive water described above (pH 8).
- In small (6/4mm) diameter tubes higher flow velocities can be permitted than in larger ($\geq 16/14$ mm) diameter tubes.

CHAPTER III

EXPERIMENTAL PROCEDURE

3.1 Experimental Approach

In the present work an experiment was designed and performed to focus on the erosion rates of Glidcop Al-15 due to varying water velocities. The specimens to be examined were four tubes made of Glidcop Al-15, which were nickel plated on the outside so as to avoid weight changes due to handling and environmental effects. A schematic of the Glidcop specimen is shown in Figure 3.1. The properties of the material under consideration are given in Table 3.1. Four samples were machined with the same dimensions. Before the start of the experiment their weights were noted.

A weighing balance with a repeatability of 0.1 mg was used to record the weights of the samples. It is shown in Figure 3.2. The balance was first installed by choosing a location free from excessive air currents, corrosives, vibration, temperature, and humidity extremes and on a level work surface. The pan and the windshield were then installed and the power was connected. The balance was then allowed to stabilize. Before actual weighing, the balance was calibrated with a 500 mg weight. Each time before weighing the balance was leveled and calibrated. The samples were handled with hand gloves in order to avoid weighing errors. The samples were placed in the same orientation each time. The weighing chamber was kept clean each time before weighing.

The test was begun by inserting these samples in a water flow system. The test area is shown in Figure 3.3. Water flowing at 15ft/s, 20ft/s, 25ft/s and 30ft/s was circulated. It

was interrupted four times during beam shutdown in the APS for general equipment repair. Each specimen was placed in a different water velocity loop. The water temperature and inlet pressure were approximately 78°F and 125psi respectively. The flow was started on Apr 15, 2003 and was stopped on Oct 17, 2003 with water flowing for approximately 4352.6 hrs. Flow meters were attached to each water velocity loop. These are shown in Figure 3.4. Water velocities were continuously monitored and adjusted using the flow meters. The experimental set up as shown in Figure 3.3 consists of three samples for each of the four velocities. Of these three samples only one from each velocity was dismantled from the set up for analysis of erosion after a period of six months. After the completion of this time period, the flow loop was dismantled and the specimens were weighed again. The specimens were then mill cut across the length and magnified pictures were taken to study the erosion corrosion phenomena. The samples were cut longitudinally and mounted on Phenolic (a thermal setting) resin shown in Figure 3.5. The Phenolic was made by placing on a thermostatic press, polymerizing in high pressure and temperatures. After mounting, the sample was then hand ground in order to preserve the surface characteristics for micrographs. The next step was to polish with a finer grid and then the photographs under magnification were taken at four different locations across the length of the samples. These four locations are labeled E2, M, M1, E1 in Figure 3.8. Micrographs for an uneroded Glidcop sample were also taken for comparison.

3.2 Results

The difference in weights corresponding to different velocities is shown in the Figure 3.6. The initial inspection of the samples revealed that as the velocities increased the color shades on the inside of the samples grew lighter somewhat similar to the uneroded sample color shade. These observations are shown in Figure 3.7. The tubes were then cut at different places along their length and viewed in a magnification of 500X. Figure 3.6 shows that as the water velocity is increased, the difference in weights of the samples lowered.

3.3 Discussion

It should be noted that in this particular experiment the samples were set up in a water loop system with no bends. At the bends the erosion may be higher. Water enters and leaves the samples longitudinally. It does not enter or leave the samples through any bends and also surface heat flux when applied may cause changes in the erosion rates. As the weight loss in higher water velocities is lower it may be noted that corrosion effects maybe higher in higher flow velocities. The corrosion deposits would have added to the samples weight. Again it is seen from the graph that for highest flow velocity (30ft/s) the difference in weight has increased which may suggest that in comparison with the 20ft/s sample the effects of the corrosion process would have been higher than the erosion effects. Corrosion process is a chemical wear caused by the reactions of flowing water with the material of the specimen. Normally, a thin film of cuprous oxide forms on exposed copper surfaces. Glidcop Al-15 used here has 99.7% copper by weight.

The micrographs of the lower velocities look similar to the uneroded Glidcop sample in terms of the surface conditions of corrosion. There are no greater deposits of corrosion on the lower velocities but erosion has taken place. This is noticed in Figure 3.8 to Figure 3.34. The higher velocity micrographs show marked changes in the surface characteristics indicating that there might be corrosion deposits on them. Increasing amounts of corrosion deposits may be present due to higher velocities. Erosion also is higher, but a net weight gain occurred due to corrosion at higher velocities. From the micrographs, it is seen that there is a significant surface roughness at water velocities of 25ft/s and 30 ft/s. Erosion is higher in the middle of the sample with velocity 30ft/s.

Table 3.1. Properties of Material-Glidcop under Consideration

Type	Glidcop Al-15
Composition	99.85% Cu, 0.15% Al ₂ O ₃
Density	$8.9 \times 10^{-6} \text{ kg/mm}^3$
Melting Pt	1083 °C
Electrical conductivity	54 Meg S/m at 20 °C
Thermal Conductivity	365 W/mK at 20 °C

3.4 Conclusions

From the weight loss data presented in Figure 3.1, the reduction in wall thickness was estimated to be approximately 0.44×10^{-3} mm. The cumulative changes in the weights are caused due to erosion as well as corrosion effects. From the micrographs, a significant increase in the surface roughness is seen for the sample with water velocity 30ft/s. The erosion rates may depend on other factors apart from high water velocities such as surface heat flux, surface finish and water pH and chemical composition.

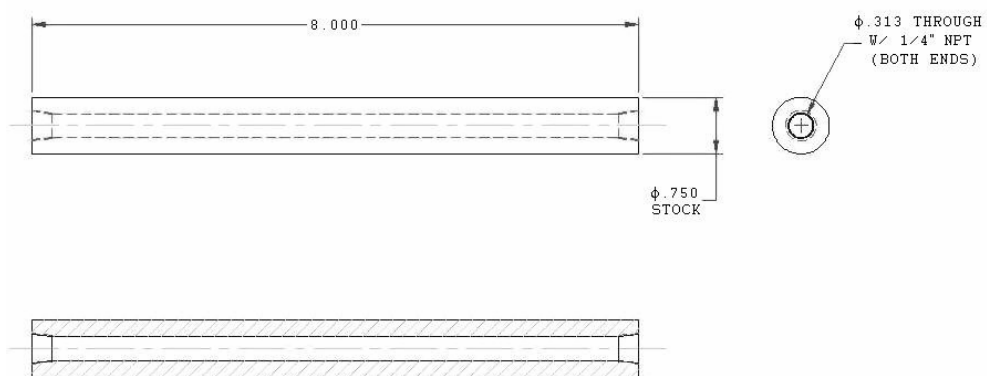


Figure 3.1. Glidcop Test Sample - Drawing

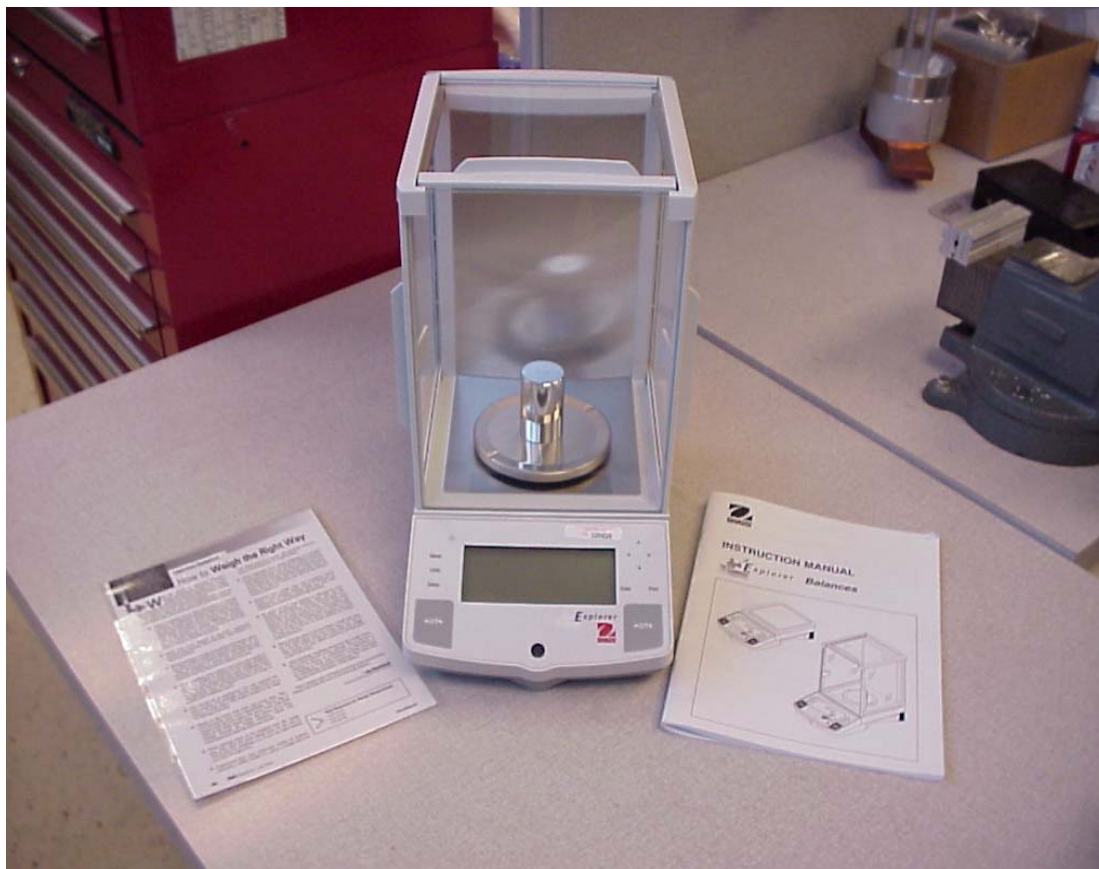


Figure 3.2. The Weighing Balance



Figure 3.3. Erosion Test Experimental Test Area



Figure 3.4. The Flowmeters



Figure 3.5. The Phenolic Mount

Sample No.	Velocities (ft/s)	Initial Weights (gms)	Final Weights (gms)	Diff in Weights (gms)
7	15	381.8483	381.8200	0.0283
4	20	379.5610	379.5336	0.0274
3	25	371.8223	371.8013	0.0210
10	30	382.2716	382.2490	0.0226

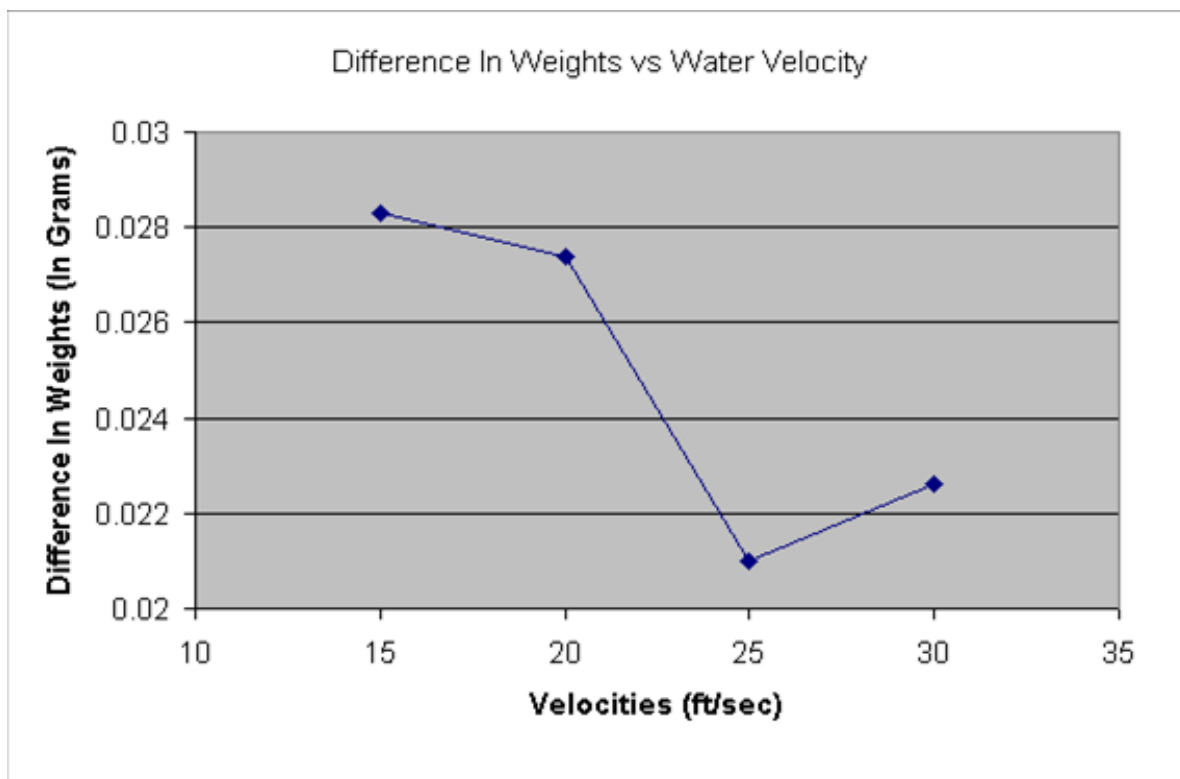
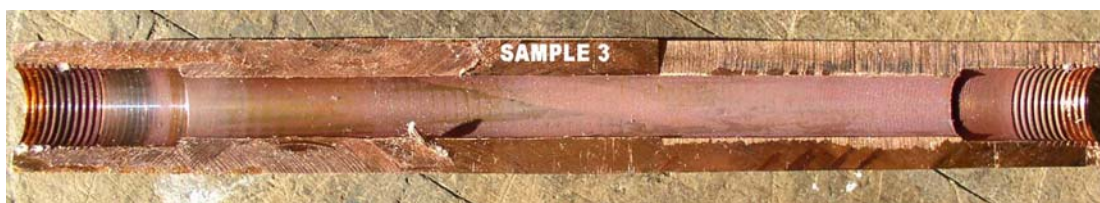


Figure 3.6. Graph of Difference in Weights in Grams vs. Water Velocities in ft/s



Sample No.10 - For Water Velocity 30ft/s



Sample No.3 - For Water Velocity 25ft/s



Sample No.4 - For Water Velocity 20ft/s



Sample No.7 - For Water Velocity 15ft/s



Sample of Uneroded Glidcop

Figure 3.7. Initial Inspection of Glidcop Samples after Mill Cutting



Figure 3.11. Micrograph of Uneroded Specimen Glidcop at end M1



Figure 3.12. Micrograph of Uneroded Specimen Glidcop at end E1



E1 M1 M E2
Figure 3.13. Sample No. 7 for Water Velocity 15 ft/s – cut pieces



Figure 3.14. Sample No. 7 for Velocity 15 ft/s micrograph at 500X at end E1



Figure 3.15. Sample No. 7 for Velocity 15 ft/s micrograph at 500X at end M1



Figure 3.16. Sample No. 7 for Velocity 15 ft/s micrograph at 500X at end M



Figure 3.17. Sample No. 7 for Velocity 15 ft/s micrograph at 500X at end E2



E1 M M1 E2

Figure 3.18. Sample No. 4 for Water Velocity 20 ft/s cut pieces of the Specimen



Figure 3.19. Sample No. 4 for Velocity 20 ft/s Micrograph 500X at end E1



Figure 3.20. Sample No. 4 for Velocity 20 ft/s micrograph 500X at end M

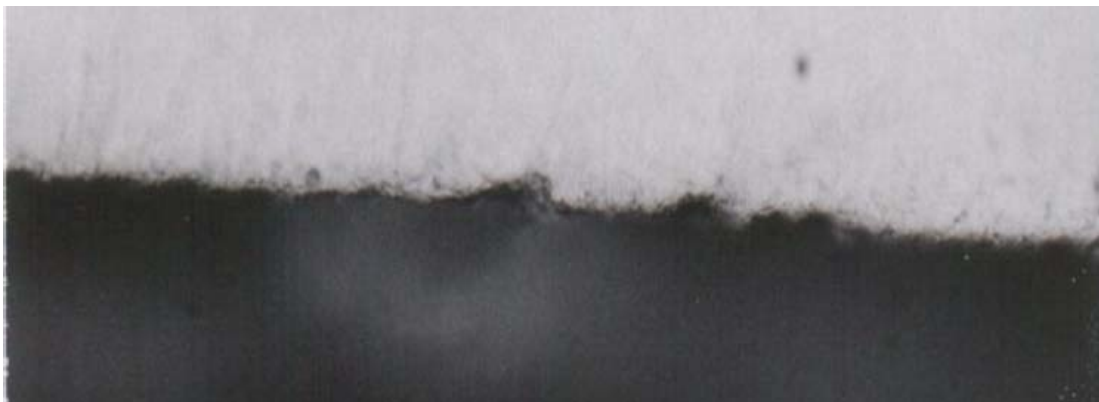


Figure 3.21. Sample No. 4 for Velocity 20 ft/s micrograph 500X at end M1



Figure 3.22. Sample No. 4 for Velocity 20 ft/s micrograph 500X at end E2



E1

M1

M

E2

Figure 3.23. Sample No. 3 for Water Velocity 25 ft/s cut pieces of the Specimen



Figure 3.24. Sample No. 3 for Velocity 25 ft/s micrograph 500X at end E1



Figure 3.25. Sample No. 3 for Velocity 25 ft/s micrograph 500X at end M1



Figure 3.26. Sample No. 3 for Velocity 25 ft/s micrograph 500X at end M



Figure 3.27. Sample No. 3 for Velocity 25 ft/s micrograph 500X at end E2

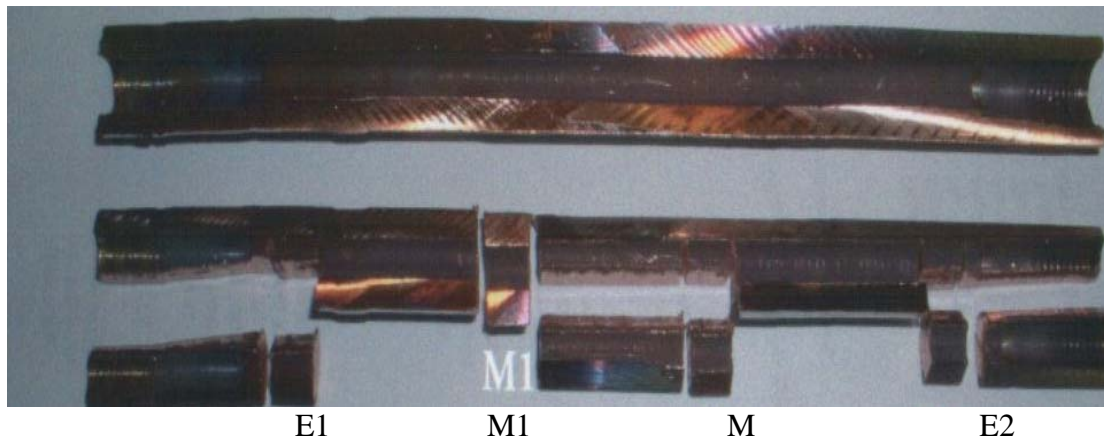


Figure 3.28. Sample No. 10 for Water Velocity 30 ft/s cut pieces of the Specimen



Figure 3.29. Sample No. 10 for Velocity 30 ft/s micrograph 500X at end E1



Figure 3.30. Sample No. 10 for Velocity 30 ft/s micrograph 500X at end M1



Figure 3.31. Sample No. 10 for Velocity 30 ft/s micrograph 500X at end M



Figure 3.32. Sample No. 10 for Velocity 30 ft/s micrograph 500X at end E2



Figure 3.33. Sample No. 10 for Velocity 30 ft/s micrograph 500X at end E2 Etched



Figure 3.34. Sample No. 10 for Velocity 30 ft/s micrograph 100X at end E2 Etched

CHAPTER IV

FINITE ELEMENT SIMULATION

4.1 Objective

The objective of the finite element analysis is to obtain the temperature distribution in Glidcop specimens subjected to a nonuniform heat flux distribution applied to one surface as a function of cooling water velocity. The finite element results are needed for future work that will involve predicting the thermal fatigue life of Glidcop specimens.

4.2 Problem Formulation

4.2.1 Geometry: A test specimen of the material Glidcop was modeled with Ansys 7.1. The dimensions of the specimen are 101.6 mm x 101.6 mm in the x - y plane with a depth of 30.7 mm in the z direction. Note that the z -axis points into the plane of the paper. The grooves are 3.2 mm x 5.2 mm in the y - z plane. There are four such grooves in the specimen. A bore with a diameter of 12.7 mm runs through the entire height of the specimen along the y -axis. The overall geometry of the specimen includes a length of 101.6 mm along the x -axis, a breadth of 30.7 mm along the z -axis a height of 101.6 mm along the y -axis.

But a single block of the model shown in Figure 4.1 is used for the analysis. The test specimen is shown in Figure 4.2. The dimensions of the single block are 101.6mm x 22.2 mm in the x and y planes and 30.7 mm in the z plane. The dimensions of the block are the same as that of a single groove of the Glidcop specimen as shown in

Figure 4.3. The experimental set up is shown in the Figure 4.4. The specimen set up is shown in the Figure 4.5. The Figure 4.6 shows the drawings of the specimen.

4.2.2 Boundary conditions: The boundary conditions for the analysis are shown in Figure 4.1. A nonuniform heat flux distribution which depends on the x and y coordinates is applied. A forced convection boundary condition is applied at the bore of the specimen through which water flows [13]. As the specimen is in vacuum all other boundaries are considered insulated.

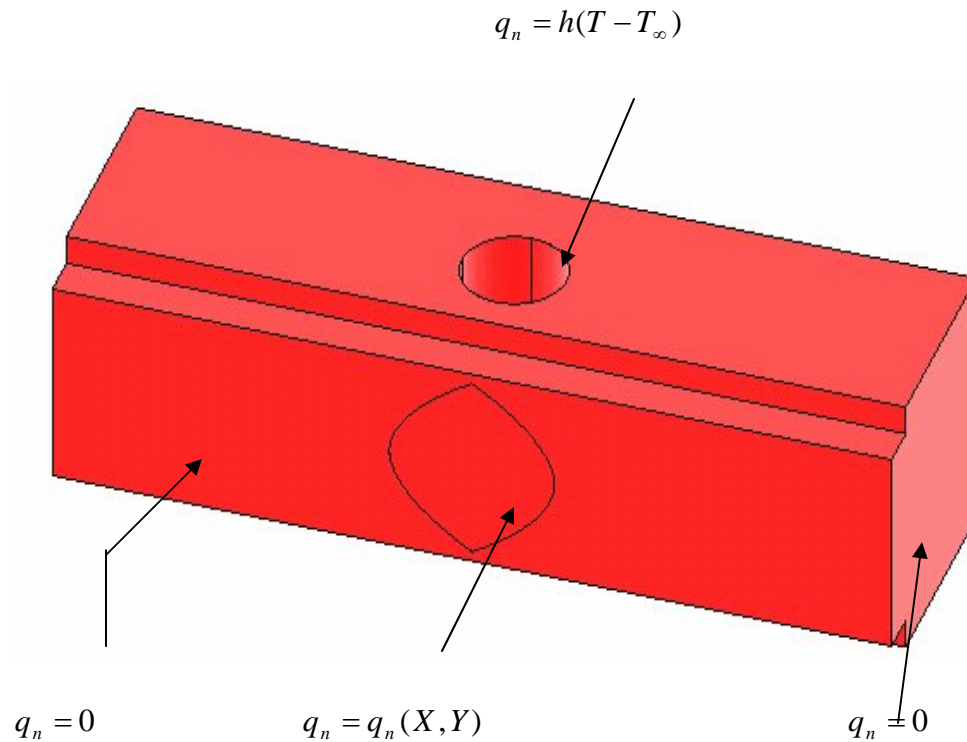


Figure 4.1. The Boundary Conditions Applied on the Glidcop Specimen

A variable heat flux due to 100mA beam current is applied in the shape of a beam footprint on one face of the block. The equation for the variable heat flux is obtained from the power density calculations of the undulator [22].

The power density for an undulator source varies both vertically and horizontally. The equations for the power density distributions can be found in reference [24]. The total power P_T can be written as

$$P_T [kW] = 0.633 E_r^2 [GeV] B_0^2 [T] L [m] I [A] \quad (4.1)$$

where E_r is the storage ring energy, B_0 is the peak magnetic field, L is the device length, I is the particle beam current.

To simulate heat transfer due to water flowing through the bore hole, a forced convection boundary condition was applied to the surface of the bore. The film coefficient varies with water velocity. The parameters for obtaining the heat flux as well as the applied film coefficient are given in Appendix A. The material properties are given in the Table 4.1.

Table 4.1. Material properties of the Analysis Material Glidcop Al-15

Property	Value
Thermal Conductivity	0.365 W/mm K
Specific Heat	391 J/Kg K
Density	8.9×10^{-6} kg/mm ³

The analysis was carried out using Ansys 7.1. The element type employed was a 4-node tetrahedral heat transfer element. In the numerical calculations, heat transfer by radiation was neglected, and the bulk temperature of water flowing through the specimen was assumed to be constant $T_{\infty} = 25^{\circ}\text{C}$. The justification for these assumptions is given in the next section. The analyses were carried out for beam currents at 100mA and 300mA. The results show that it is sufficient to consider just a single block subjected to a 100mA current.

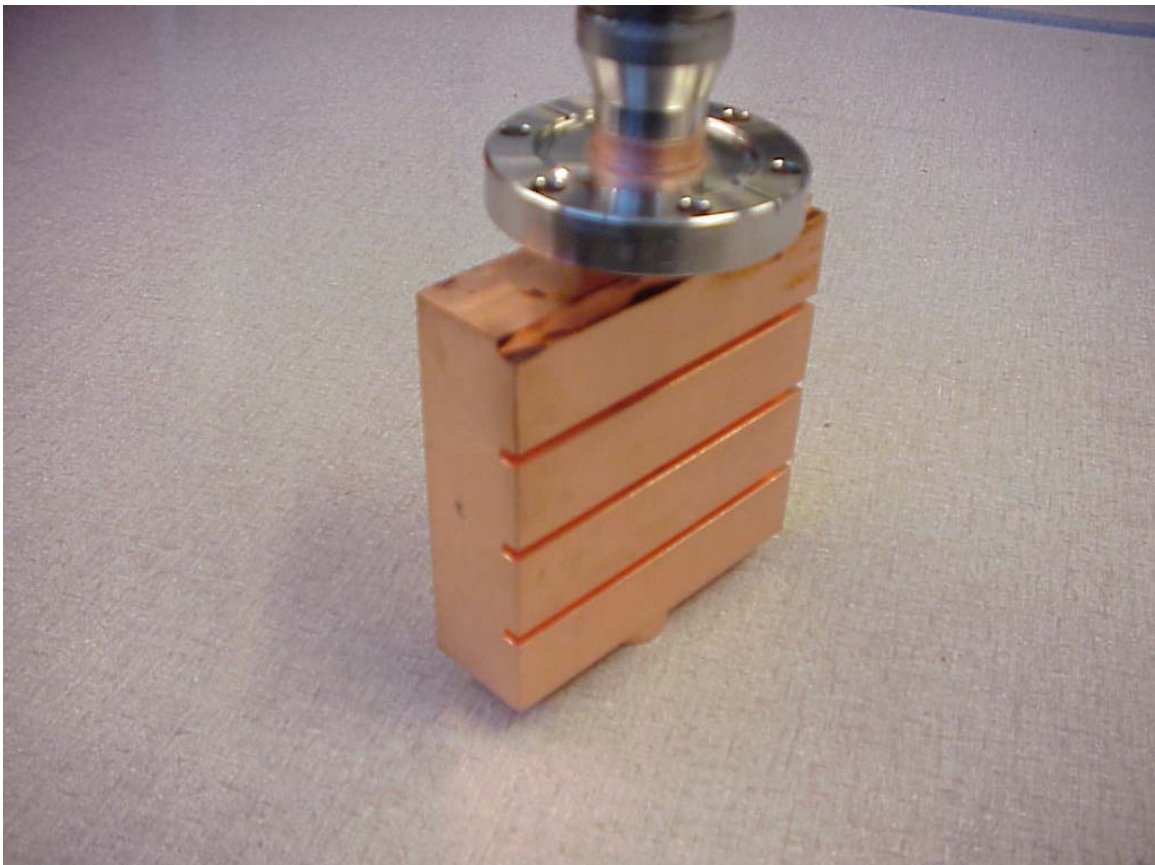
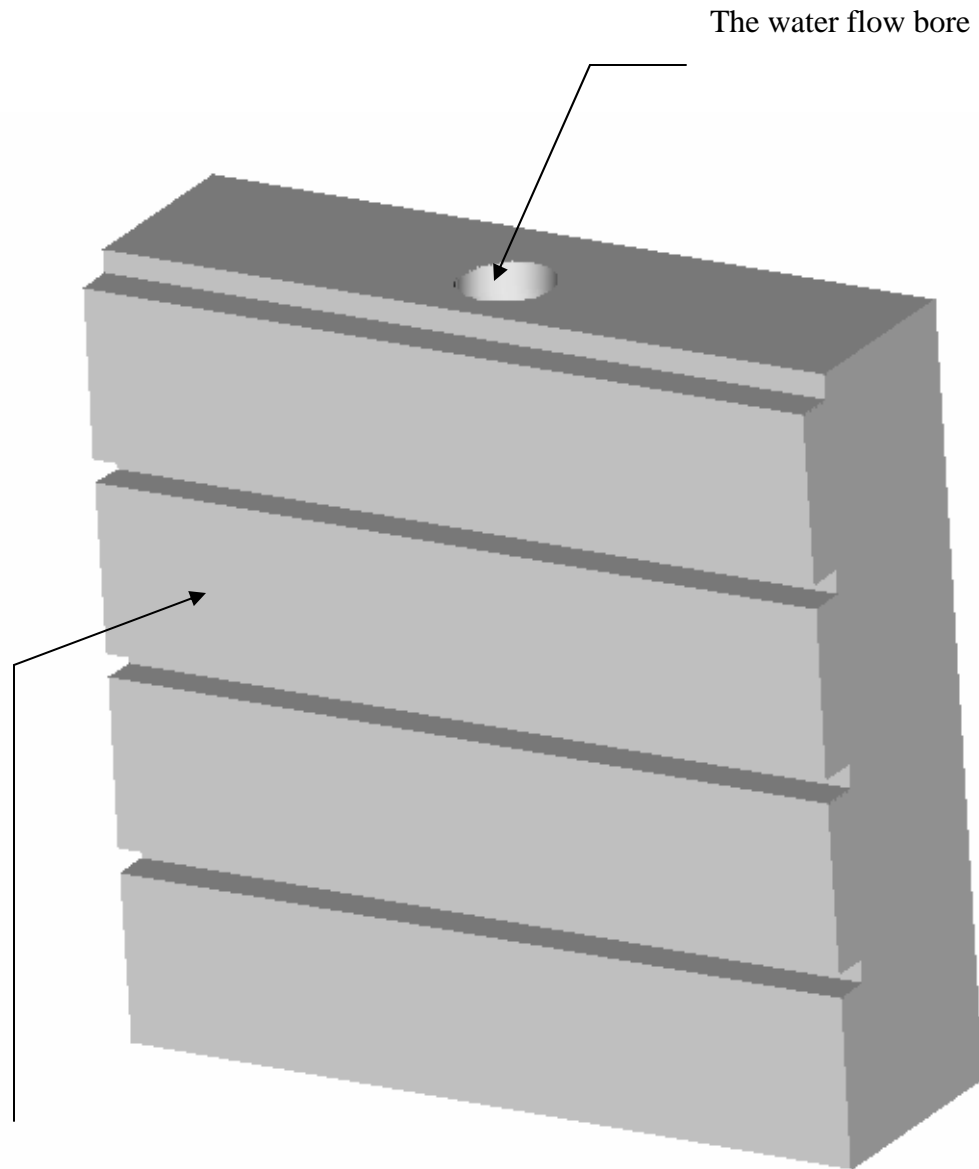


Figure 4.2. The Glidcop Analysis Test Specimen



The single block modeled

Figure 4.3. The Glidcop Specimen 101.6mm x 101.6mm modeled for the Finite Element Analysis

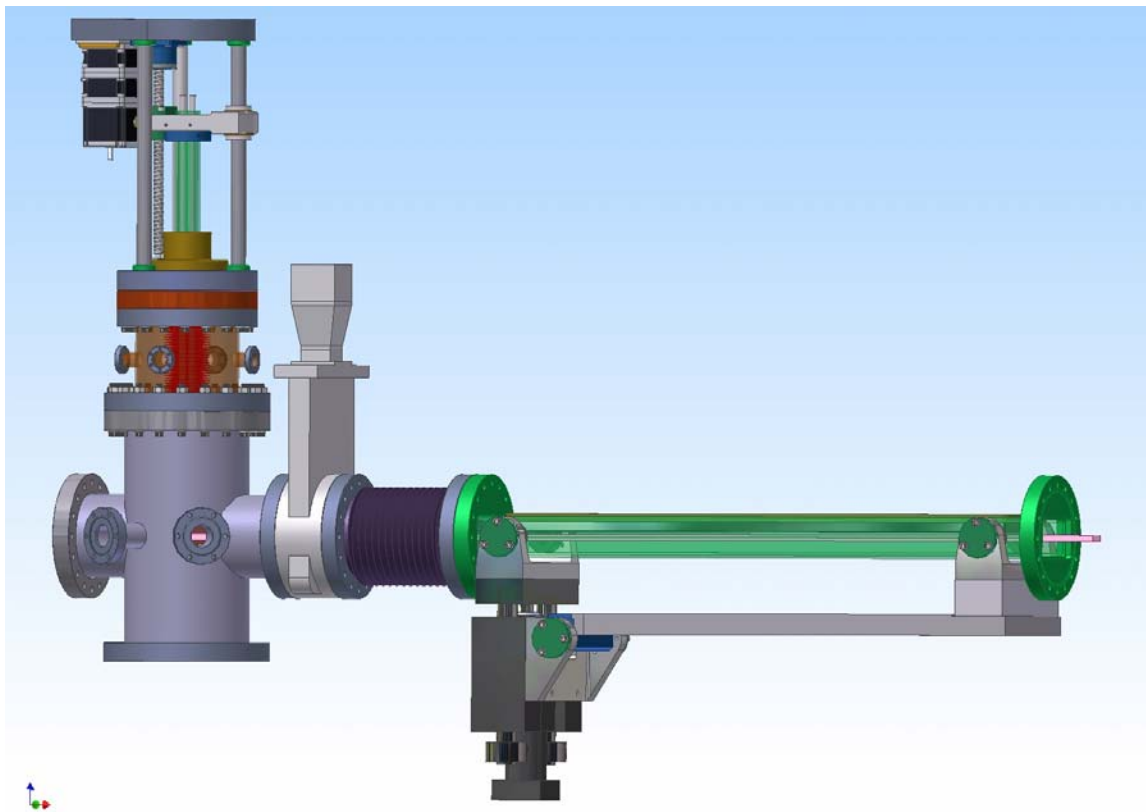


Figure 4.4. The Glidcop Test Station

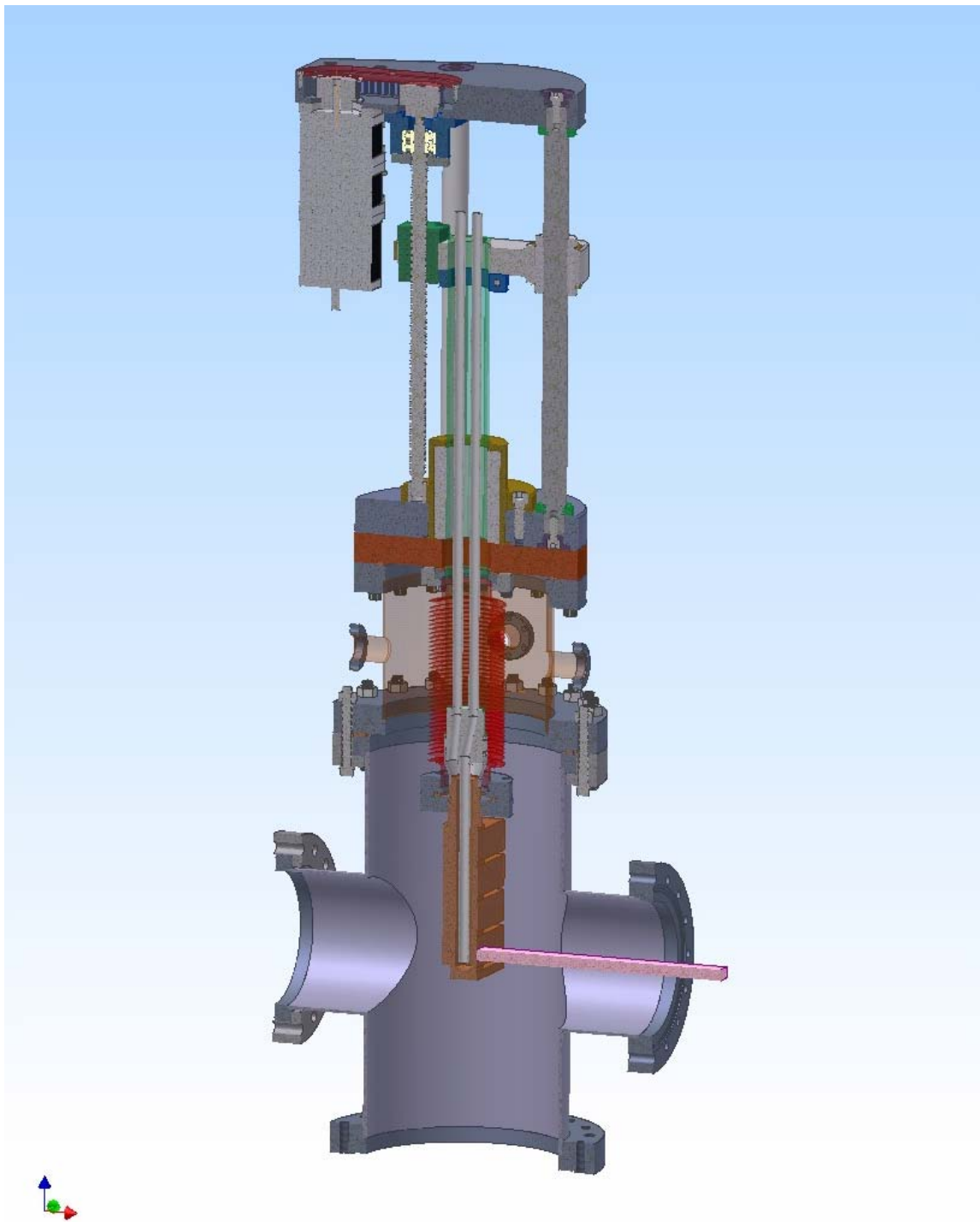


Figure 4.5.The Glidcop Test Station 2

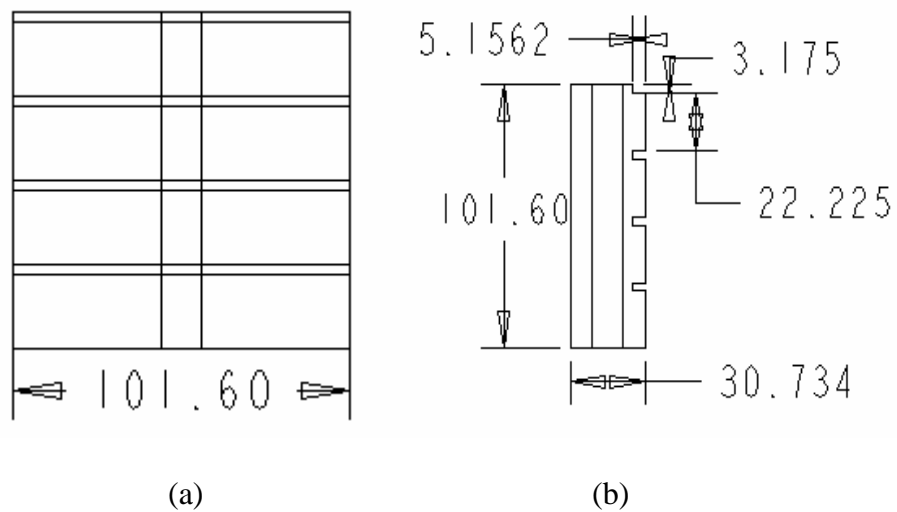


Figure 4.6. (a). Front View of the specimen, (b). Side View of the specimen

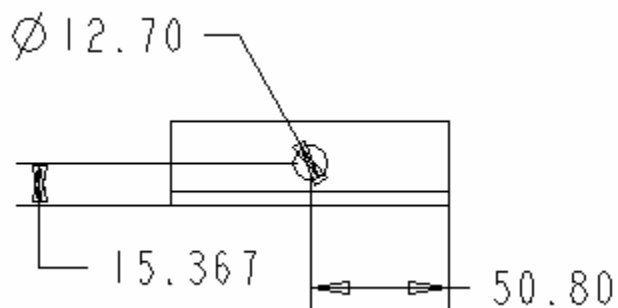


Figure 4.6 (c). The Top View of the Specimen with a Bore Hole of Diameter 12.7mm

4.3 Numerical Results

Table 4.2. Peak Temperatures Vs Velocities for 100mA and 300mA Beam Current

Velocity (ft/sec)	Peak Temp for 100mA	Peak Temp for 300mA
10	344.549	983.525
15	338.115	964.227
20	334.340	952.905
25	331.755	945.153
30	329.835	939.394

From the Table 4.2 it is seen that by increasing the beam current to 300mA, the steady state peak temperature rise is three times. The loads are applied as shown in Figure 4.7.

The analysis for both beam currents is shown in Figure 4.8 and Figure 4.9.

Figures 4.8 and Figure 4.9 show, as expected, that the temperature distribution scales linearly with beam current. Therefore, it was not required to perform the analysis for 300mA beam current. A simpler model with a single block instead of the whole block (Glidcop sample) and with 100mA beam current was considered for the remainder of the analysis as shown in Figure 4.10.

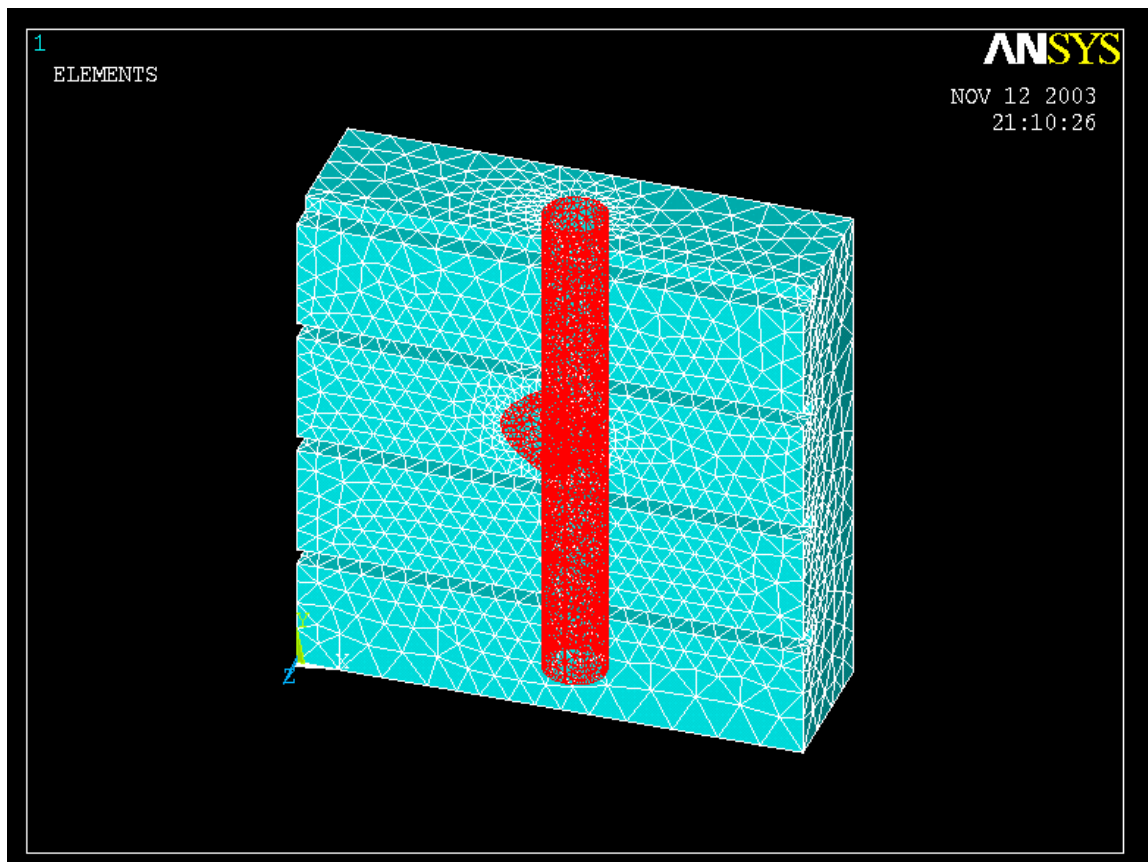


Figure 4.7. For 100mA and 300mA Beam Current the Loads Applied

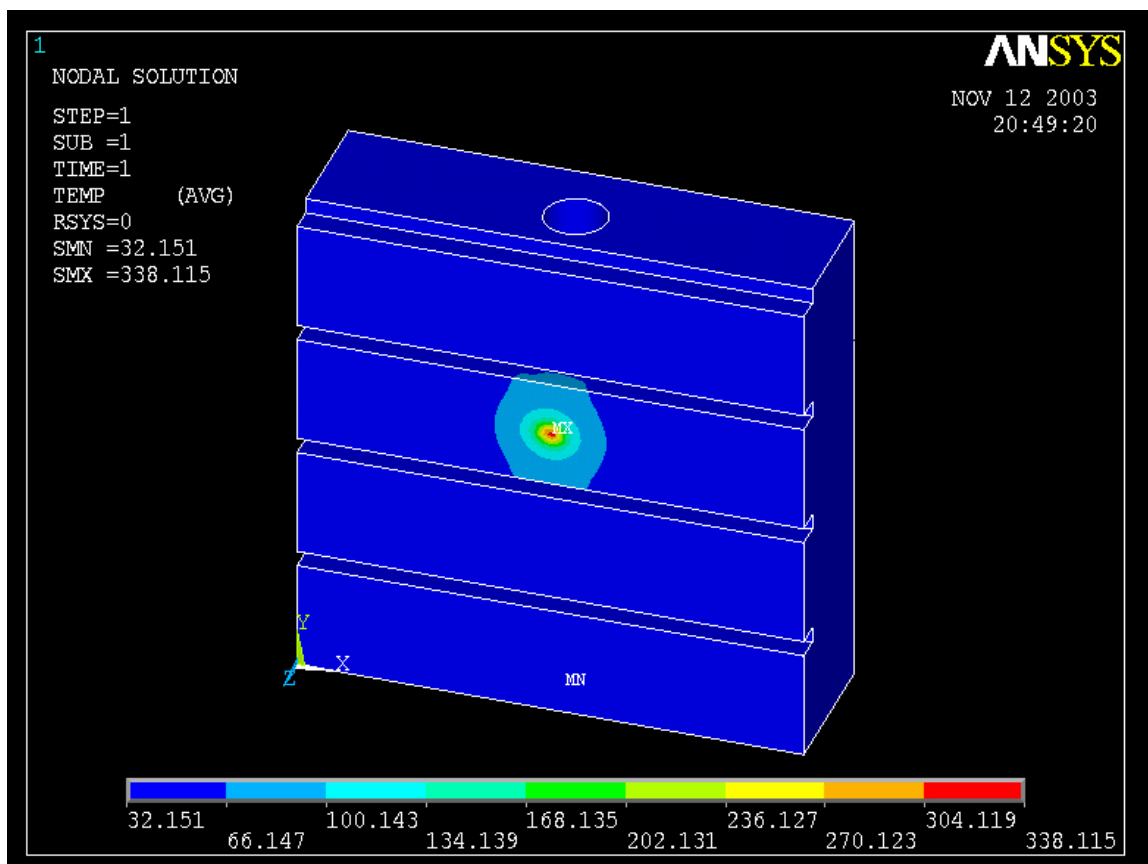


Figure 4.8. For Water Velocity 15ft/sec – 100mA Beam Current

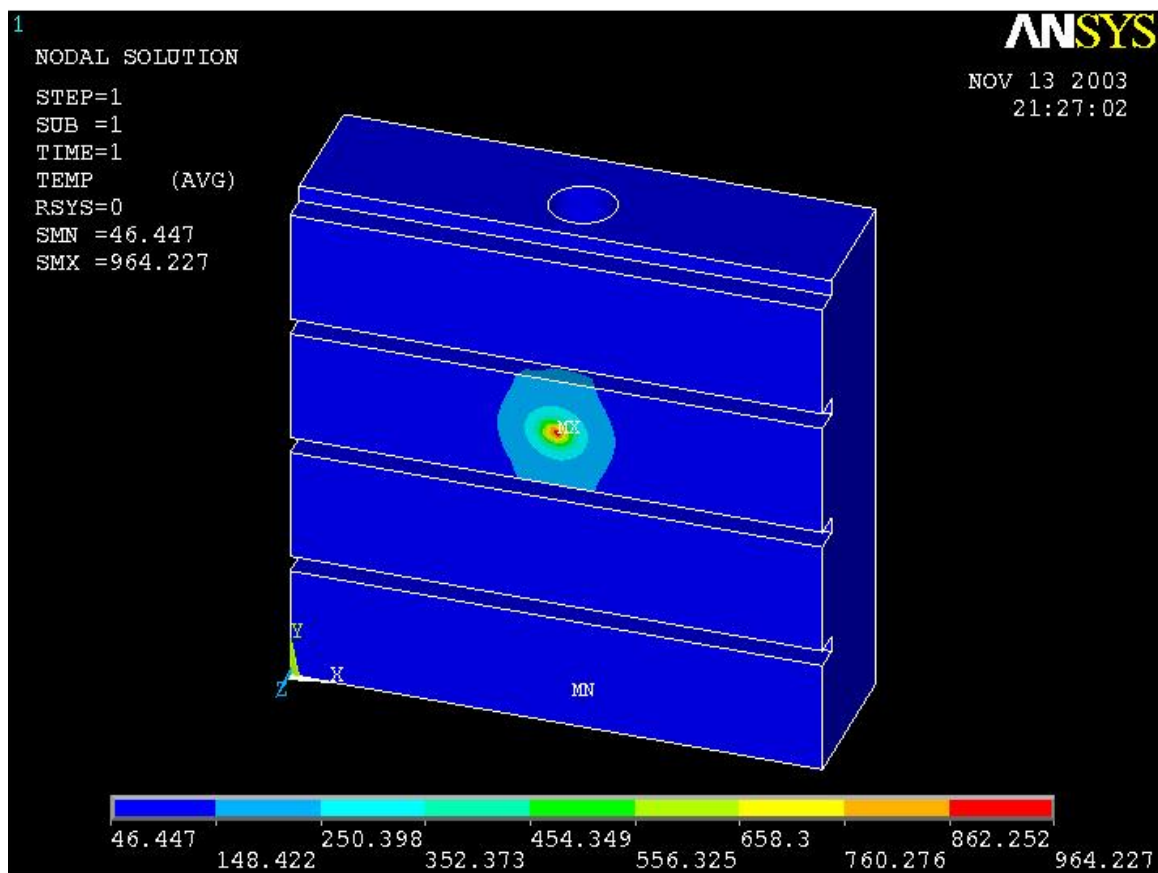


Figure 4.9. For Water Velocity 15ft/sec – 300mA Beam Current

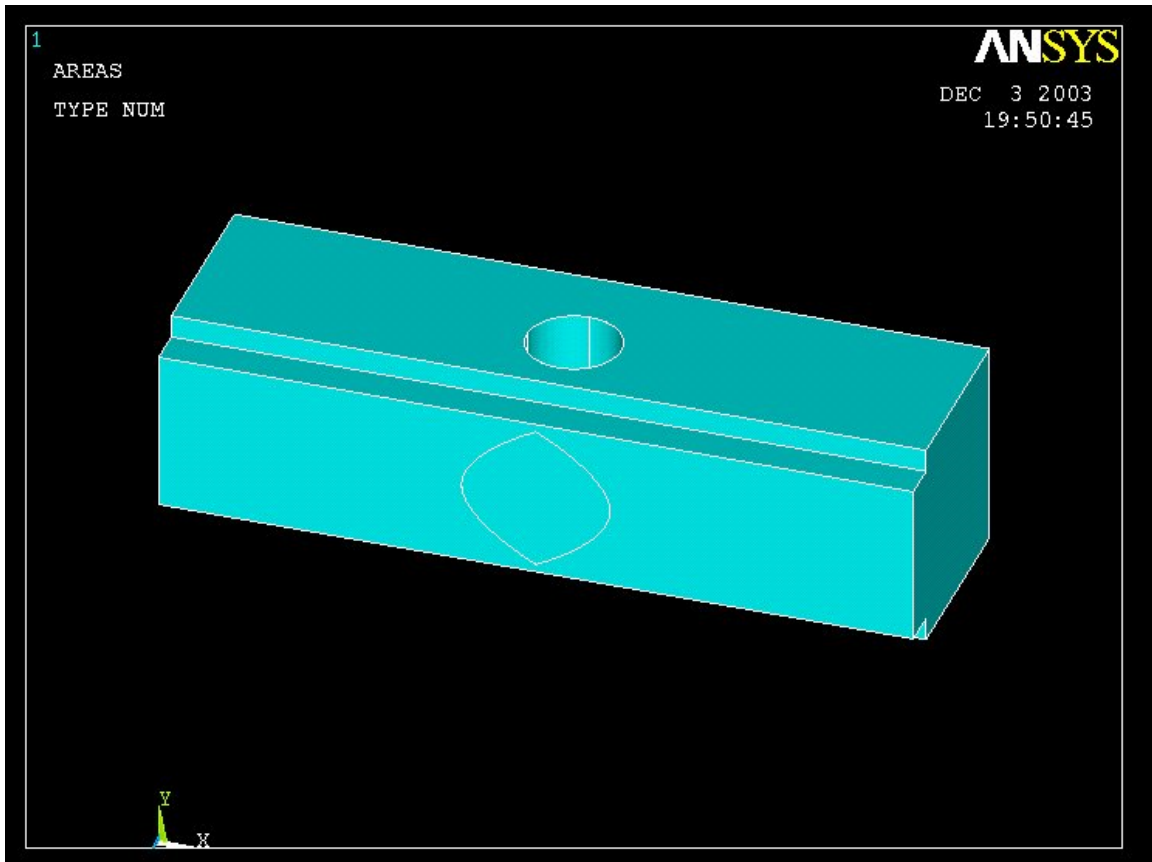


Figure 4.10. The Single Block Specimen which is Modeled for the Analysis.

The results for the single block analysis and for the 100mA beam current are presented in Figure 4.11 and Figure 4.12. The peak temperature in the block with the present beam current of 100mA and water flow velocity 5ft/s was found to be 438.2 °C.

Table 4.3 gives the peak temperature values for varying flow velocities. The temperature at the surface of the bore was found to be well below 100⁰ C, hence the water is not expected to boil. Figures 4.13 to Figure 4.24 give the steady state and transient analysis results. The Table 4.4 gives the transient analysis values.

Given the flow velocity and the diameter of the bore hole, the film coefficients were obtained from [21] and Appendix C and are listed in Table 4.3.

Table 4.3. Peak Temperatures of the steady state analysis with varying velocities

Temp Range °C	Velocity (ft/s)	Film coefficient (W/mm ² °C)
128.098-438.189	5	0.00645
79.617-387.683	10	0.01123
61.964-368.463	15	0.01553
52.734-357.946	20	0.01955
47.048-351.166	25	0.02338
43.213-346.386	30	0.02705

Single Block

Velocity(ft/s)	5	10	15	20	25	30
Peak Temp *C	438.189	387.683	368.463	357.946	351.166	346.386
FilmCoeffW/mm2*C	0.00645	0.01123	0.01553	0.01955	0.02338	0.02705

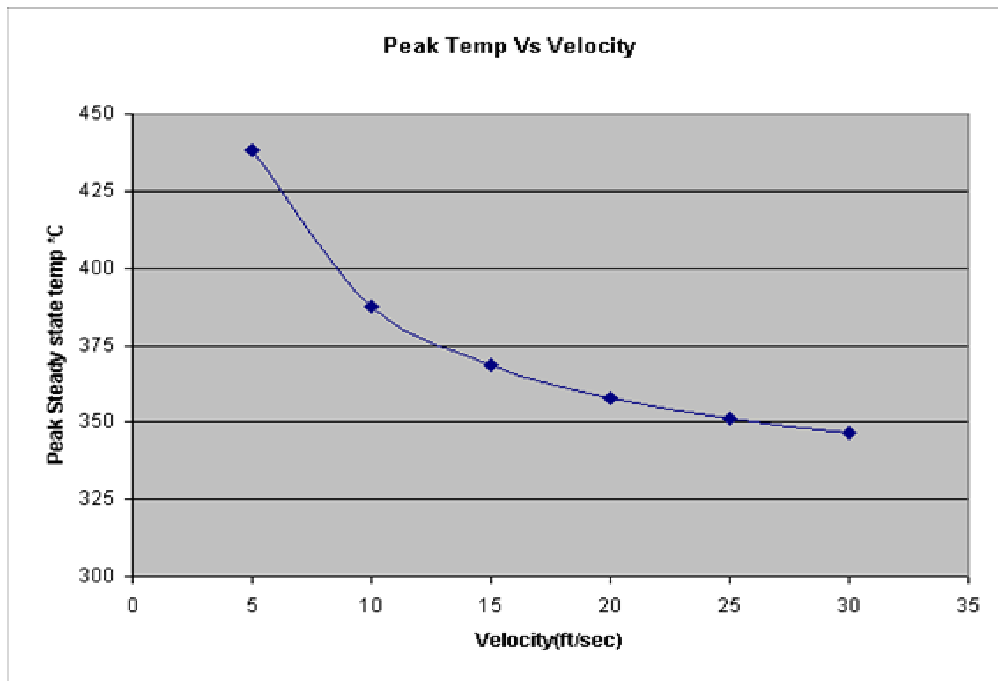


Figure 4.11. Graph of Peak Temp for 100mA Beam Current vs. Velocity of Water

Single block model

Film Coefficient ($\text{W}/\text{mm}^2\text{ }^\circ\text{C}$)	0.00645	0.01123	0.01553	0.01955	0.02338	0.02705
Temp Rise $^\circ\text{C}$	438.189	387.683	368.463	357.946	351.166	346.386
Velocity (ft/s)	5	10	15	20	25	30

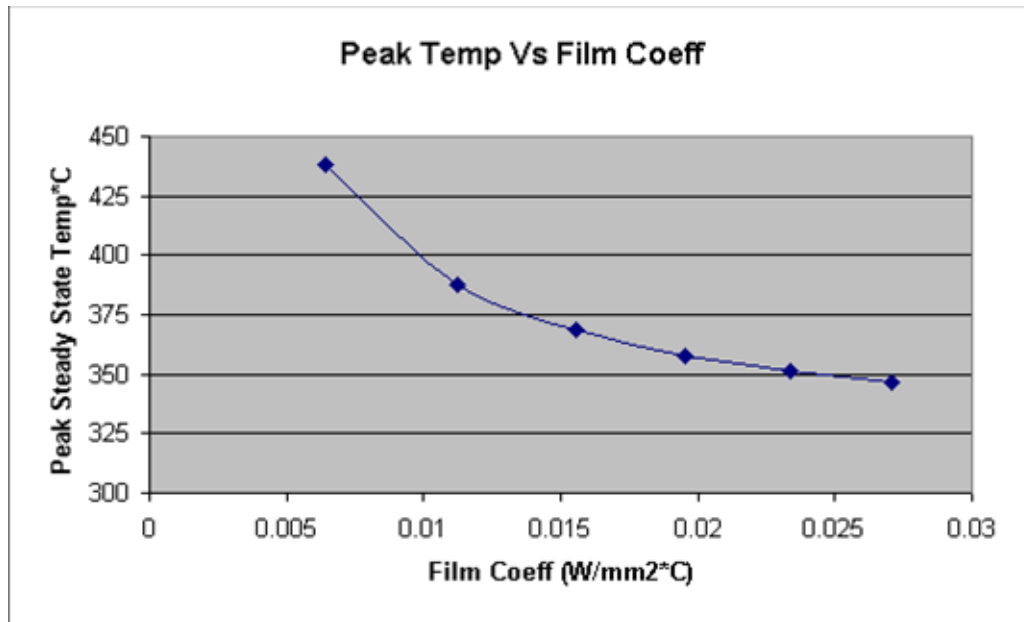


Figure 4.12. Graph of Peak Temp for 100mA Beam Current Vs Film Coefficient of Cooling
Water in Glidcop

It turns out that the assumption of neglecting heat transfer by radiation is justified because the difference in the temperatures between the specimen and the surroundings is relatively small. The radiative heat transfer is proportional to the fourth power of absolute temperature [25] according to Stefan's Law. If one assumes an emissivity of 0.1 and the block is assumed to be at uniform temperature of $438.2\text{ }^\circ\text{C}$ in a surrounding vacuum at $25\text{ }^\circ\text{C}$, the temperature decrease of the block during a 40 second time period (the time it takes for the block to reach steady-state) is less than $4\text{ }^\circ\text{C}$. The assumption that the

cooling water passing through the bore hole remains at 25 °C is also justified. The time that it takes for a column of water to flow through the sample is approximately 0.01 s for a flow rate of 5 ft/s. Assuming that all the power from the beam source goes into the water, the temperature rise of the column of water would be only on the order of 1 °C.

4.4 Conclusions and Future Work

The finite element analysis results for the Glidcop block reveal that when a nonuniform heat flux is applied to one surface of the block due to an X-ray beam from an undulator, the peak temperatures scale linearly with the beam current. The decrease in the steady-state peak temperatures is drastic from velocities of 5ft/sec to 15ft/sec after which the decrease in the peak temperatures is not very considerable. Also, as the surface roughness increases due to erosion of Glidcop absorbers for water velocities higher than 25 ft/sec, it was found that no considerable advantage is gained by increasing the cooling water velocity to a level higher than 25ft/sec.

Future thermal fatigue tests on Glidcop samples may require that the samples reach higher temperatures than those obtained in the above analyses in order to generate fatigue cracks. If that is the case, the fatigue tests can be performed on Glidcop by using lower water velocities to reach high temperatures rather than by increasing the beam current. Another method for obtaining a higher peak temperature in the Glidcop sample would be to move the bore hole closer to one of the ends of the block. The transient analysis provides the time that can be expected for the block temperature to reach steady-state. In the present analysis the time to

reach steady-state was found to be approximately 40 s. Further transient analyses would be required in the future if any of the conditions are changed such as moving the bore hole. The time that it takes for the block to reach steady-state dictates the controller frequency needed for the fatigue test experiments.

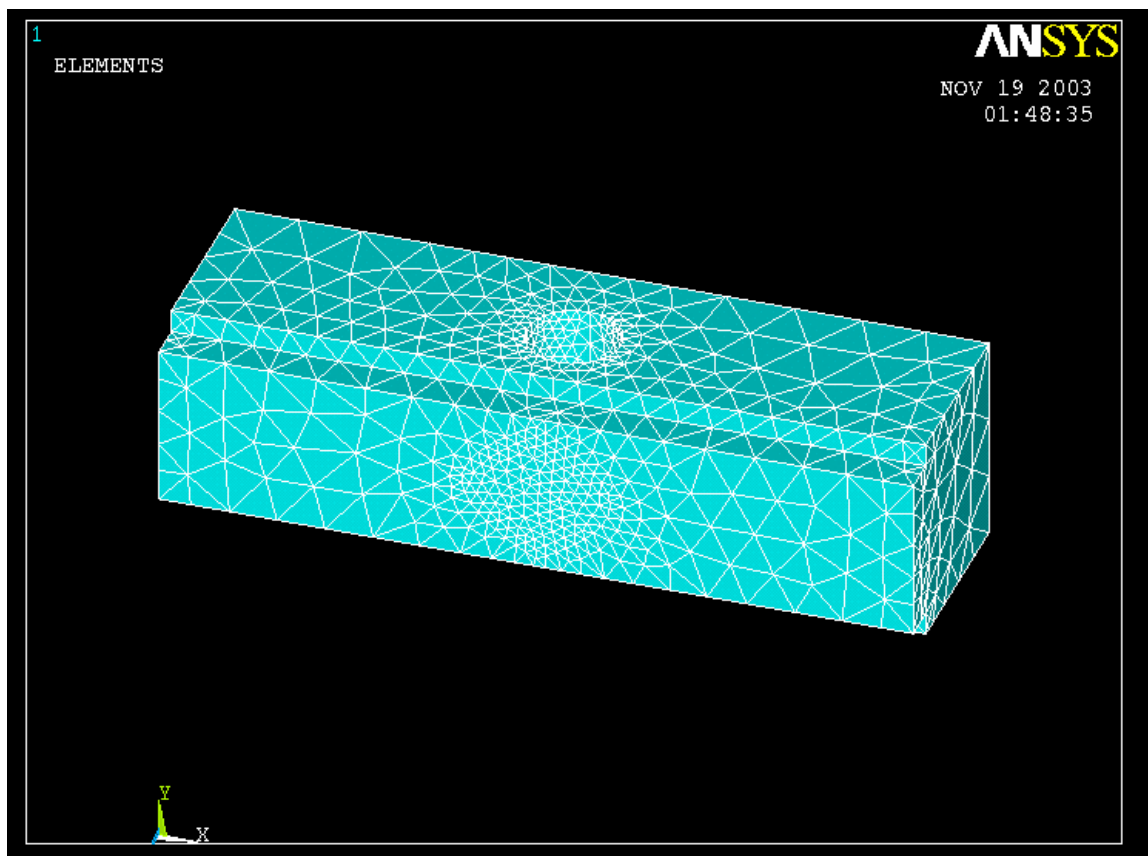


Figure 4.13. The 3D Model of the Absorber Meshed

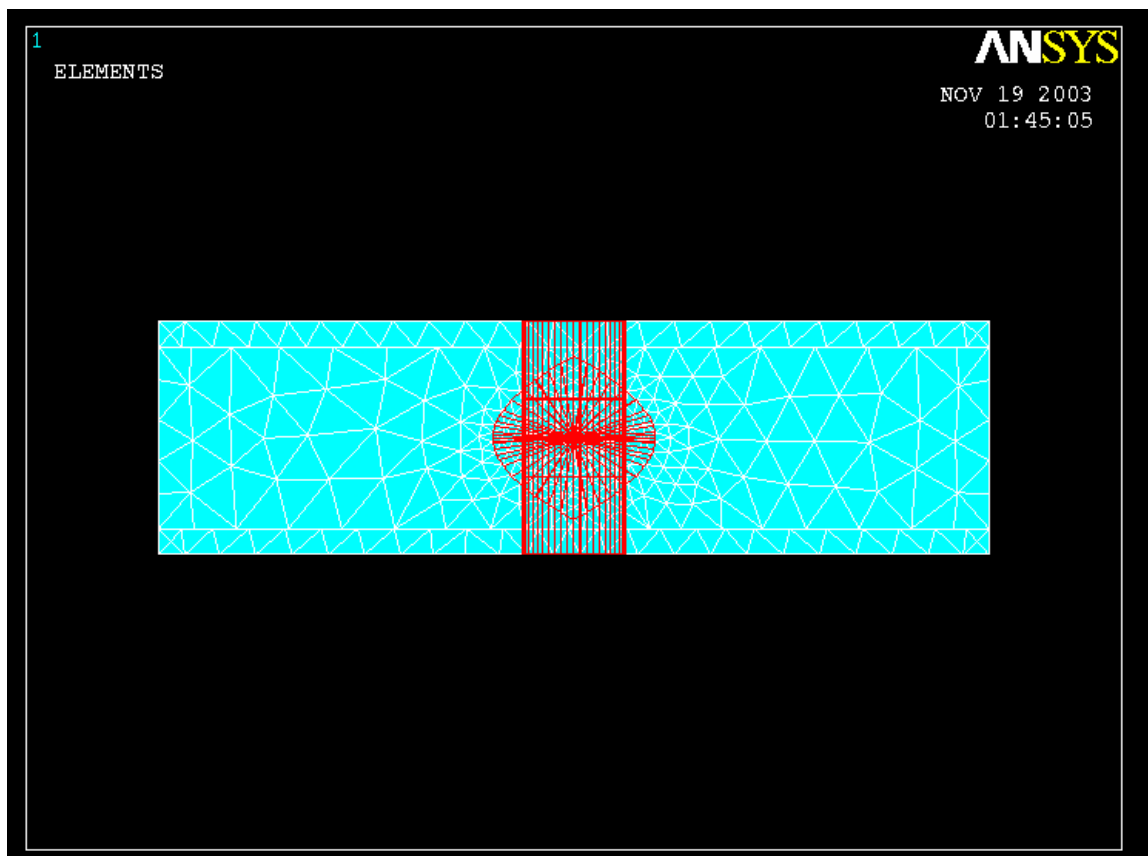


Figure 4.14. Loads on the model – Front View

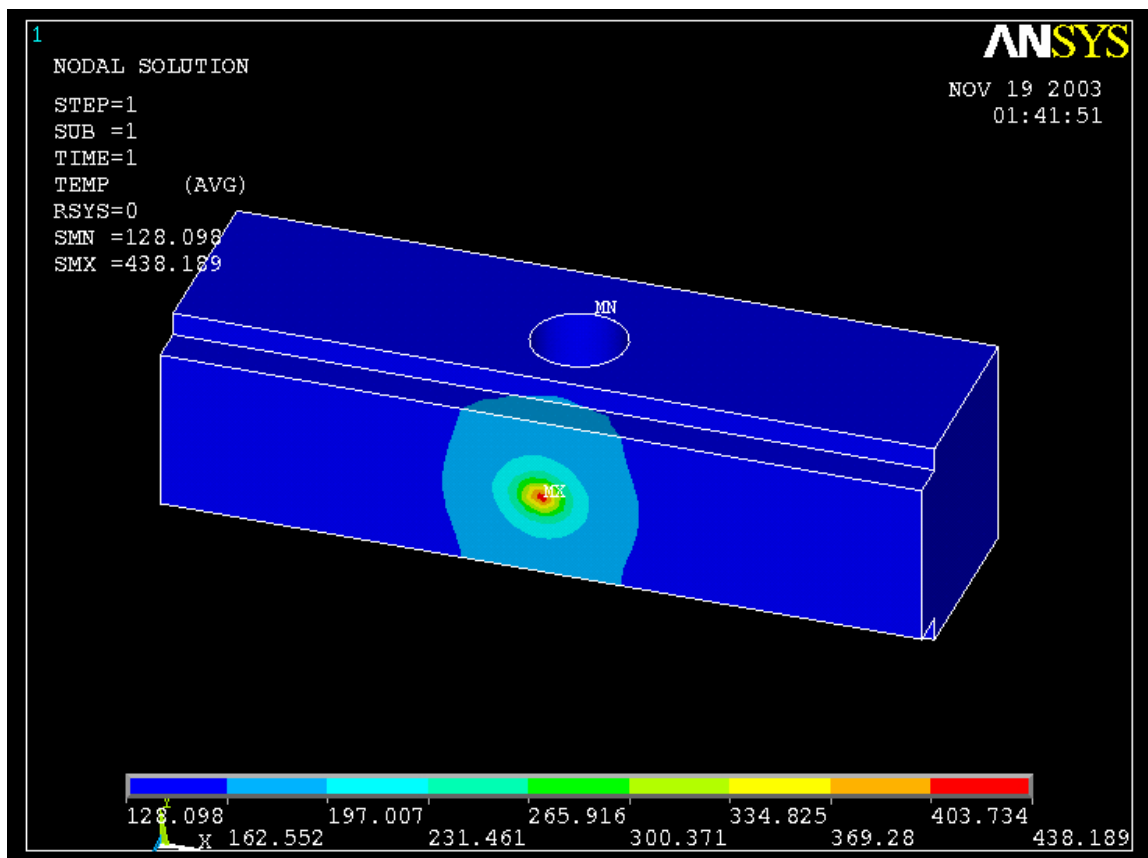


Figure 4.15. Temperature Distribution for Water Velocity – 5ft/s

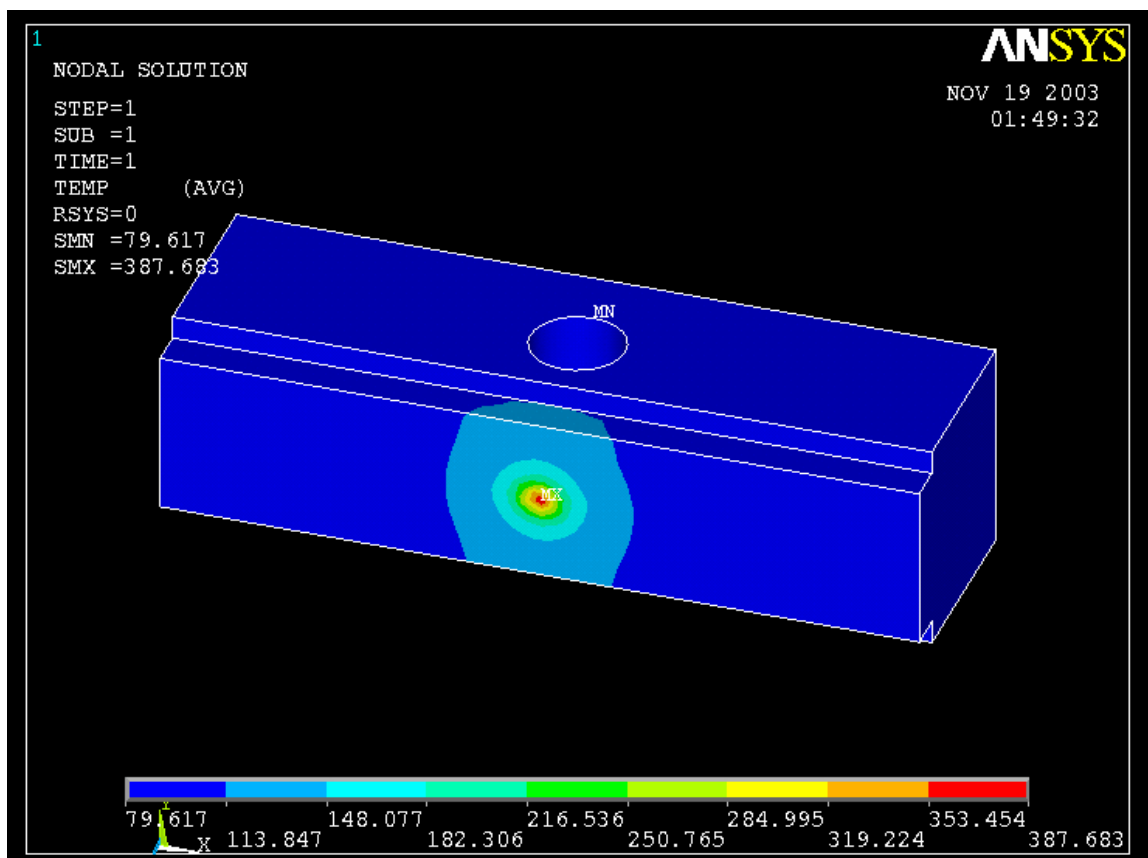


Figure 4.16. Temperature Distribution for Water Velocity – 10ft/s

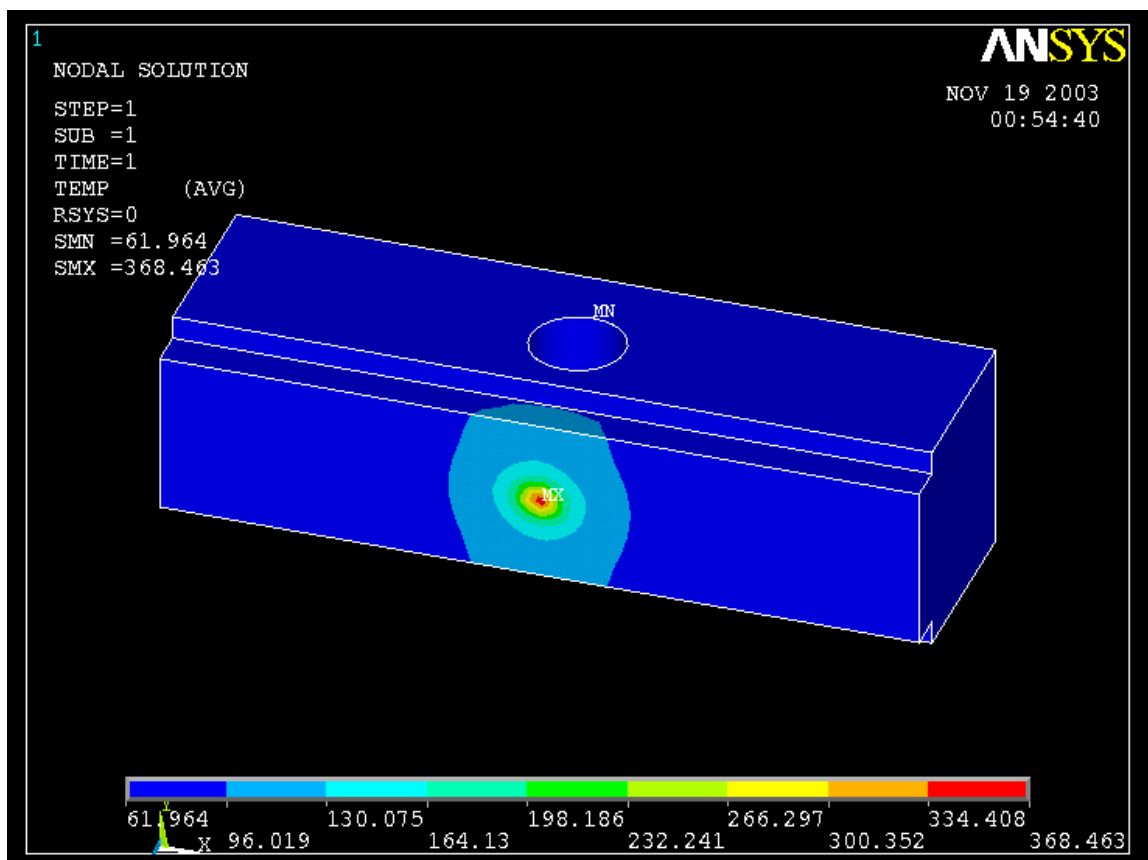


Figure 4.17. Temperature Distribution for Water Velocity – 15ft/s

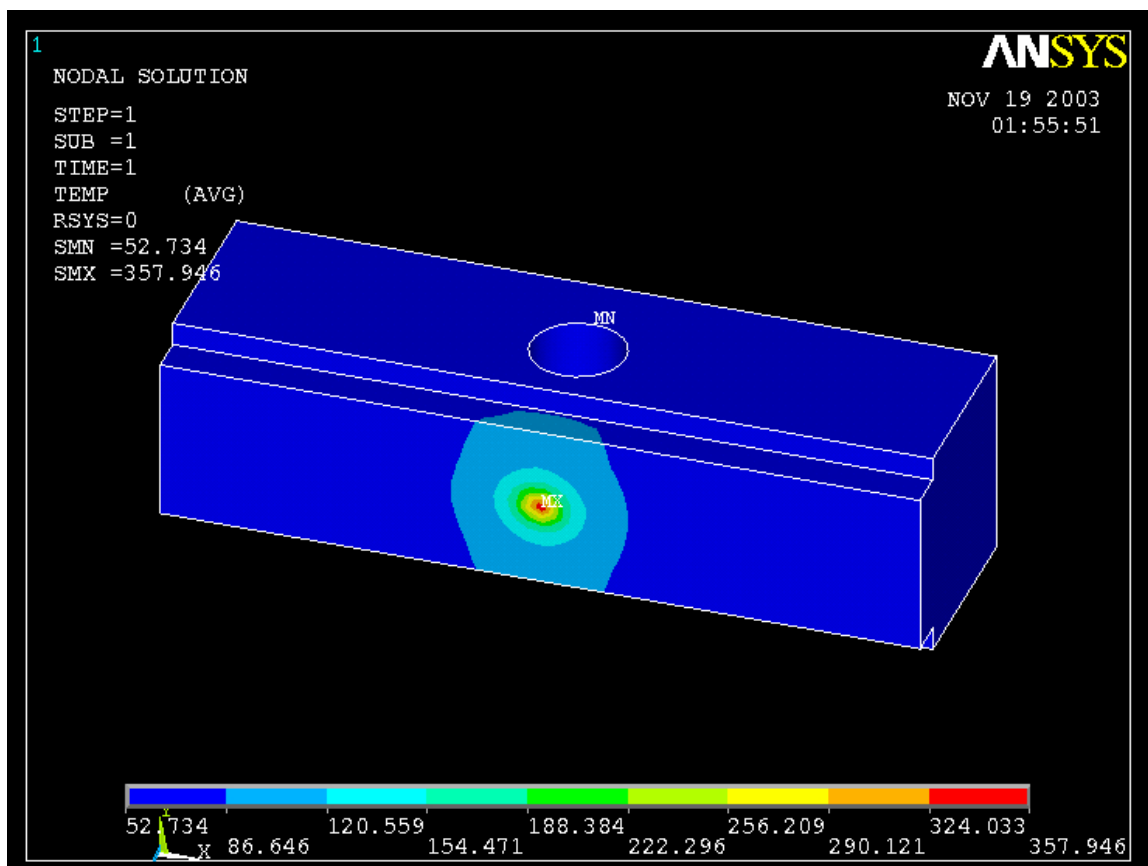


Figure 4.18. Temperature Distribution for Water Velocity – 20ft/s

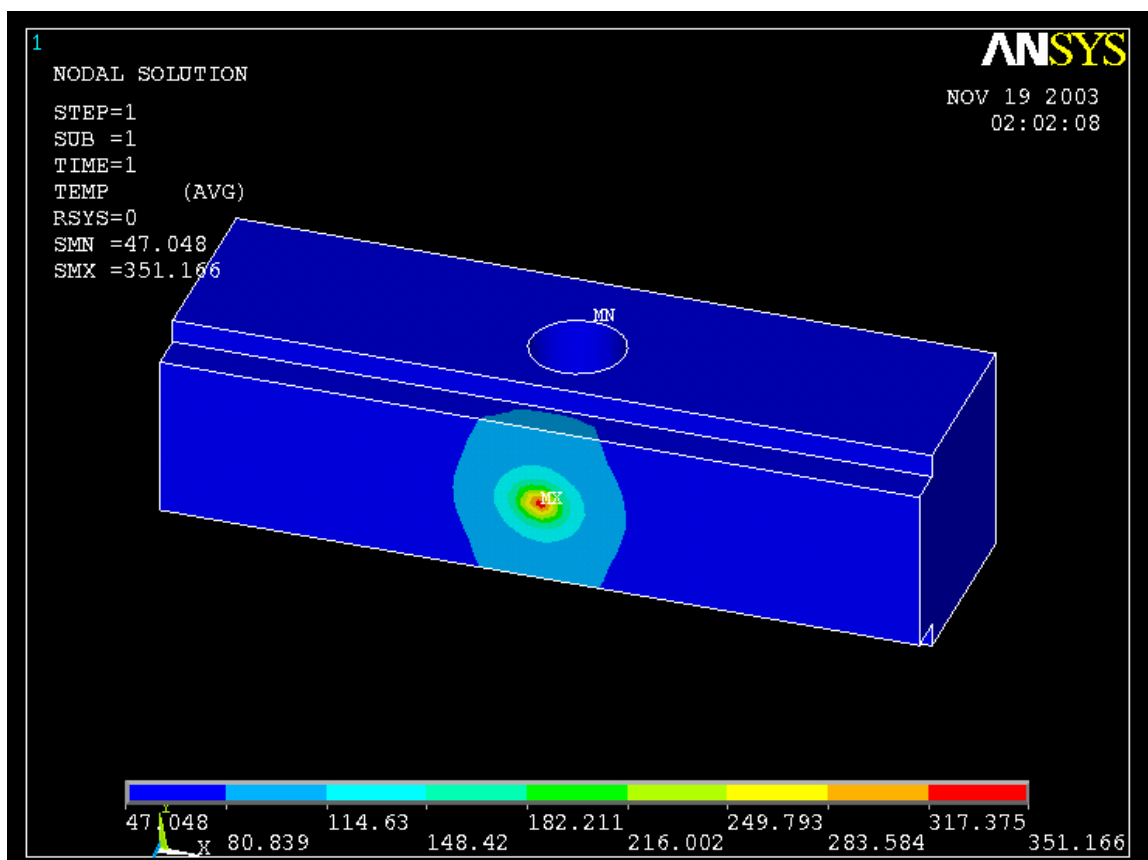


Figure 4.19. Temperature Distribution for Water Velocity – 25ft/s

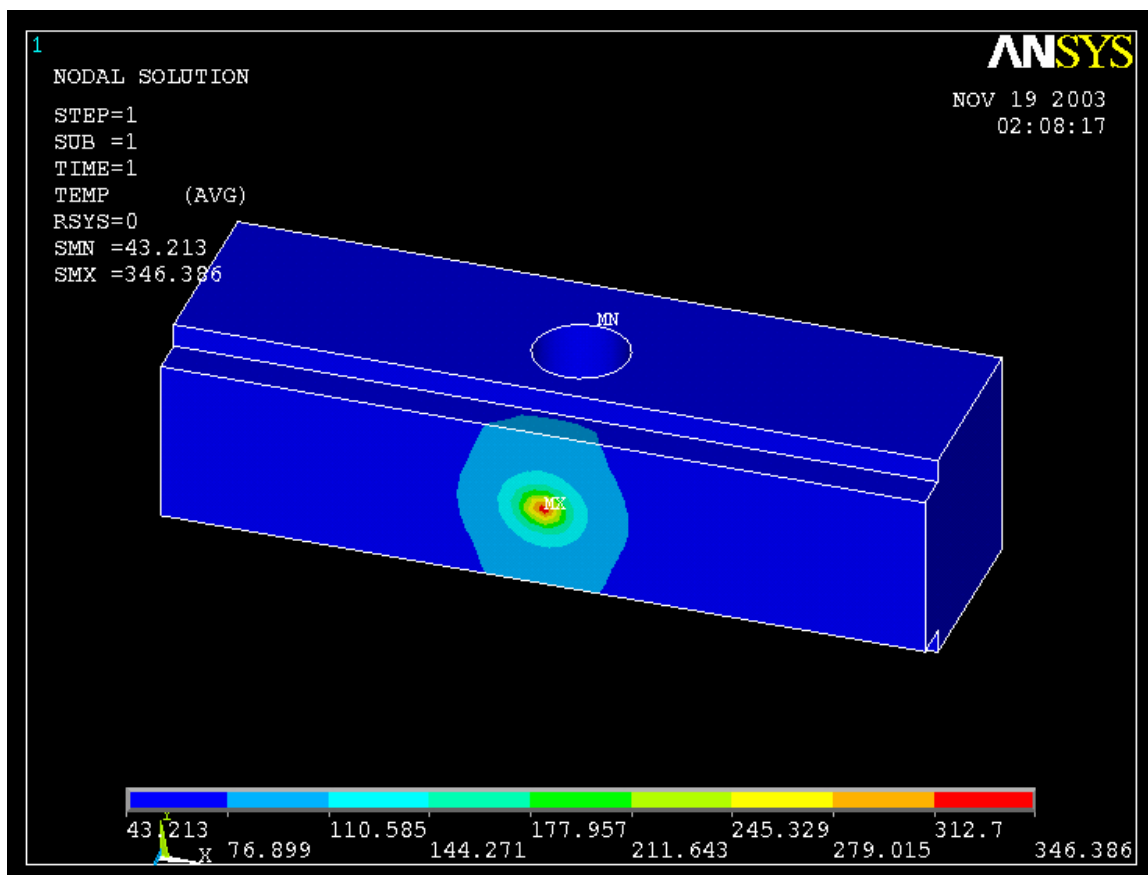


Figure 4.20. Temperature Distribution for Water Velocity – 30ft/s

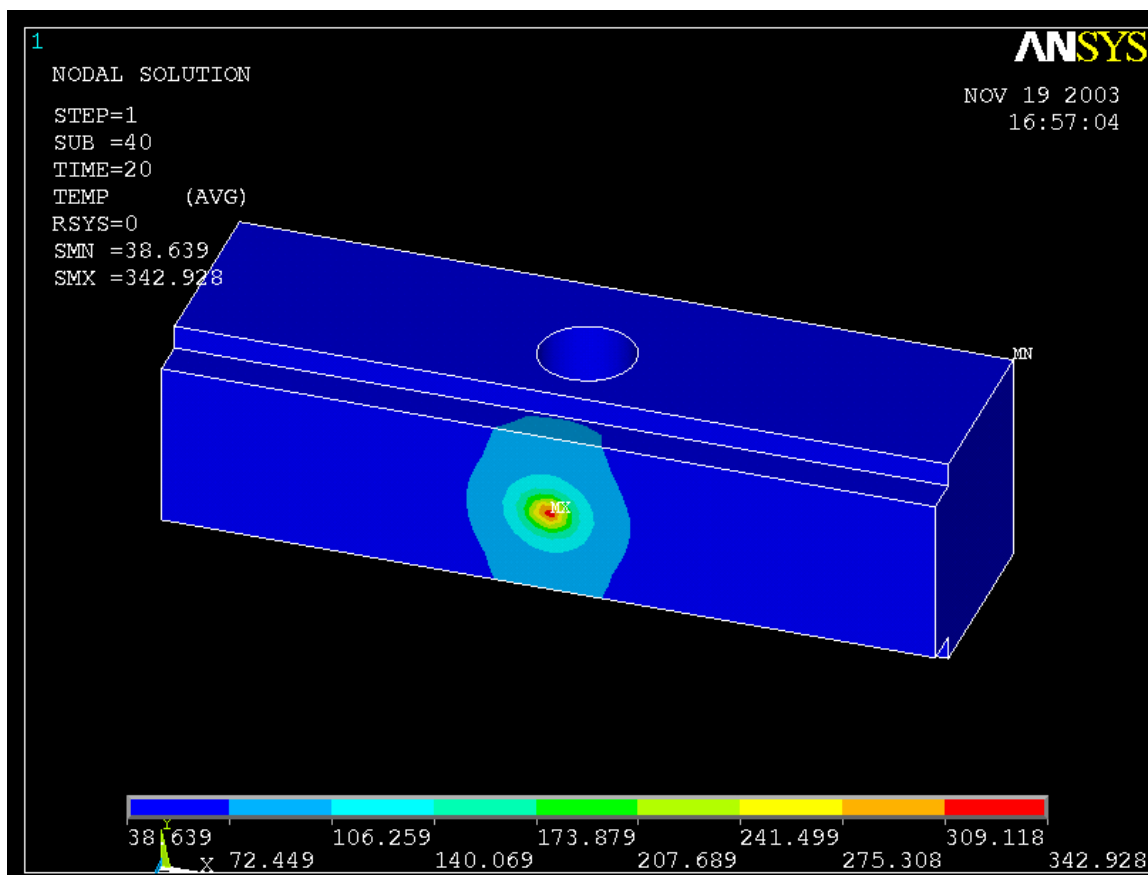


Figure 4.21. Transient analysis for 100mA and 15ft/s – 20sec, time step size 0.5

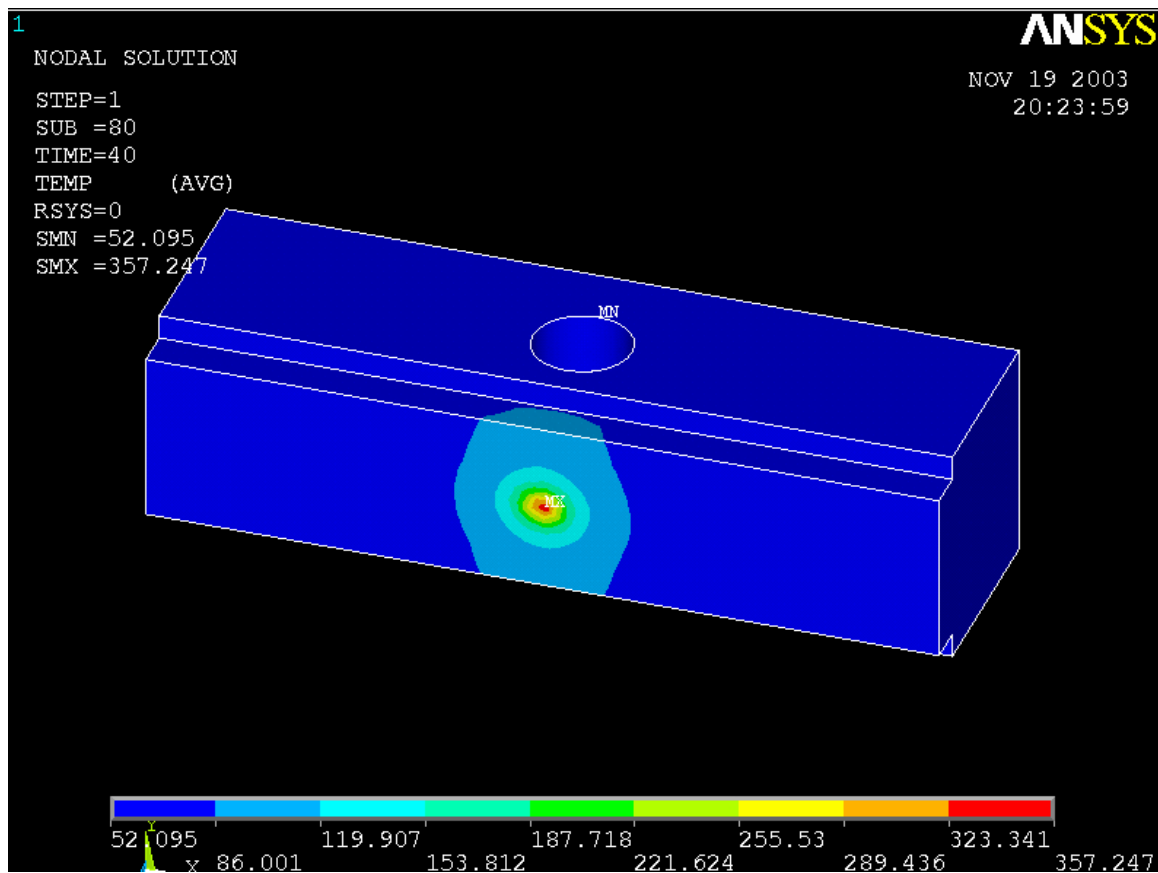


Figure 4.22. Transient analysis for 100mA and 15ft/s – 40sec, time step size 0.5

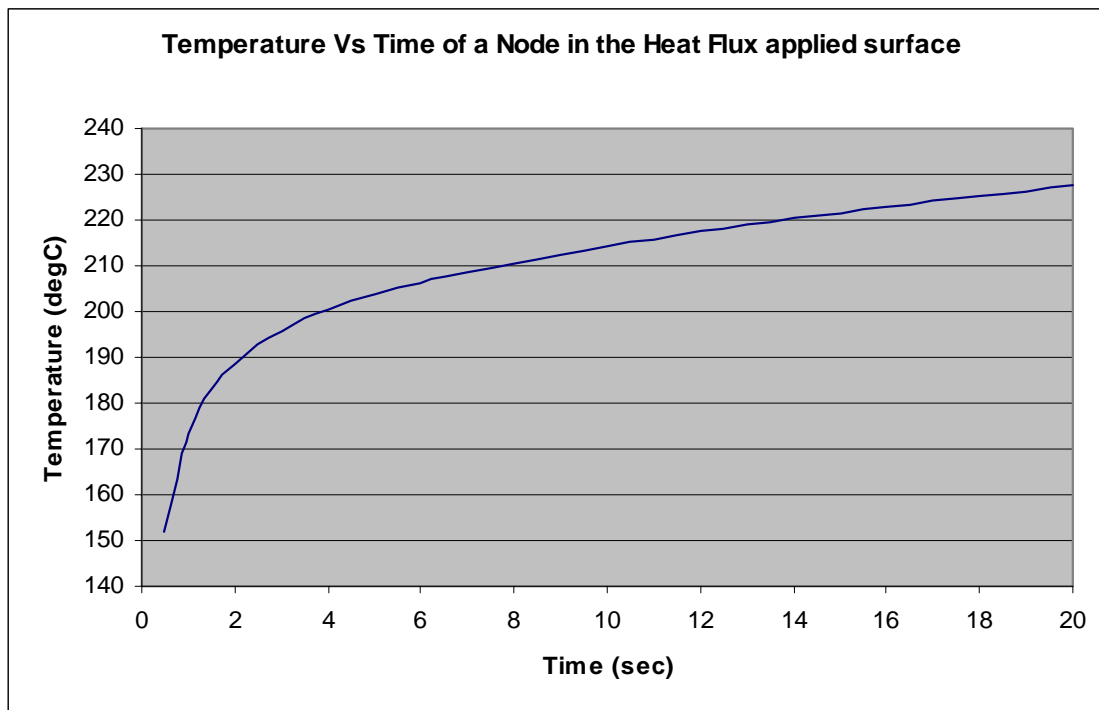


Figure 4.23. Graph of Temp_1 Vs Time of a node from transient analysis 20 sec

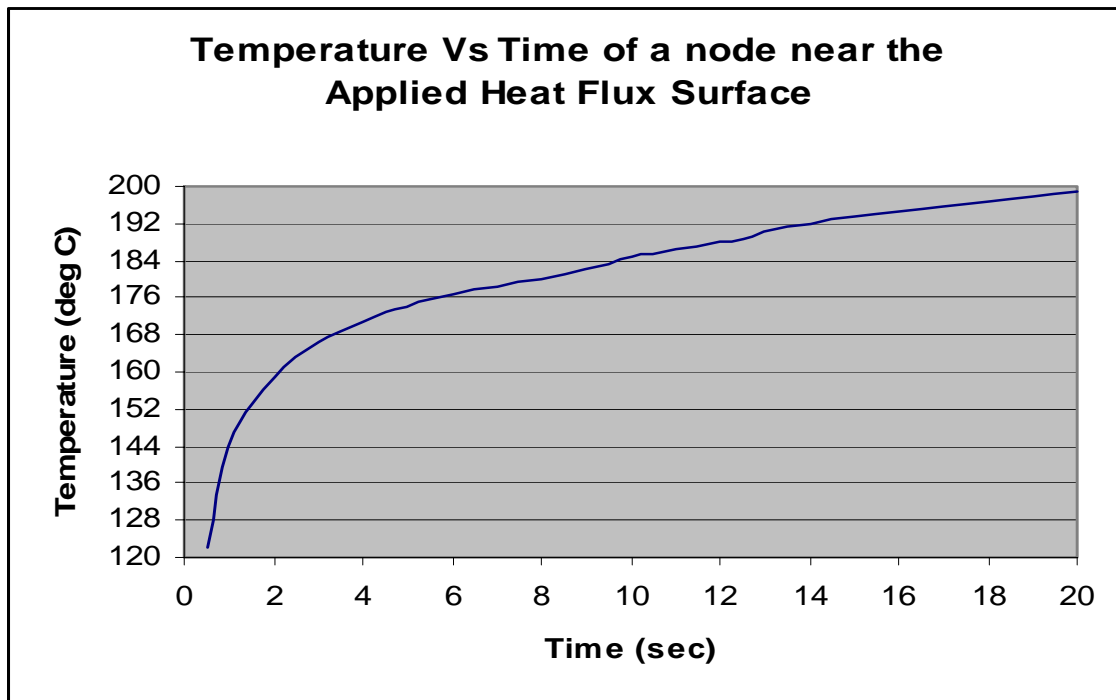


Figure 4.24. Graph of Temp_2 Vs Time of a node from transient analysis 20 sec

Table 4.4 The Values of the Transient Analysis Graphs

Time (s)	Temp_1 (°C)	Temp_2 (°C)
0.5	151.683	122.031
1.0	173.152	143.623
1.5	182.637	153.165
2.0	188.531	159.081
2.5	192.69	163.248
3.0	195.839	166.399
3.5	198.344	168.904
4.0	200.417	170.975
4.5	202.189	172.744
5.0	203.742	173.844
5.5	205.134	175.683
6.0	206.403	176.949
6.5	207.576	177.849
7.0	208.674	178.119
7.5	209.709	179.212
8.0	210.694	180.245
8.5	211.636	181.226
9.0	212.541	182.165
9.5	213.414	183.067
10.0	214.259	184.778
10.5	215.079	185.595
11.0	215.875	186.388
11.5	216.651	187.161
12.0	217.407	187.913
12.5	218.144	188.648
13.0	218.864	190.065
13.5	219.567	191.420
14.0	220.255	192.075
14.5	220.927	192.717
15.0	221.585	193.344
15.5	222.229	193.959
16.0	222.859	194.56
16.5	223.476	195.149
17.0	224.080	195.726
17.5	224.671	196.291
18.0	225.251	196.844
18.5	225.818	197.386
19.0	226.373	197.917
19.5	226.917	198.244
20.0	227.450	198.855

APPENDIX A

**ANSYS 7.1 LOG FILE FOR THE COMPUTATION OF TEMPERATURE
DISTRIBUTION IN THE GLIDCOP 3D BLOCK WITH VARIABLE
HEAT FLUX EQUIVALENT TO A BEAM OF 100mA APPLIED**

```

/BATCH
!/COM,ANSYS RELEASE 7.1  UP20030501    18:59:28  11/18/2003
!*

!/COM,ANSYS RELEASE 7.1  UP20030501    21:34:46  10/31/2003    !*
!/COM,
!/COM,Preferences for GUI filtering have been set to display:
!/COM, Thermal
!*

*DIM,HEATFLUX,TABLE,11,11,1,X,Y
HEATFLUX(0,1) =56.9125
HEATFLUX(0,2) =57.9125
HEATFLUX(0,3) =58.9125
HEATFLUX(0,4) =59.9125
HEATFLUX(0,5) =60.9125
HEATFLUX(0,6) =61.9125
HEATFLUX(0,7) =62.9125
HEATFLUX(0,8) =63.9125
HEATFLUX(0,9) =64.9125
HEATFLUX(0,10) =65.9125
HEATFLUX(0,11) =66.9125

HEATFLUX(1,0)=45.8,46.8,47.8,48.8,49.8,50.8,51.8,52.8,53.8,54.8,55.8

HEATFLUX(1,1)=0.1404,0.2171,0.3054,0.3681,0.3726,0.3579,0.3726,0.3681,0.3054,0.
2171,0.1404
HEATFLUX(1,2)=0.2412,0.4147,0.6414,0.7834,0.6422,0.4630,0.6422,0.7834,0.6414,0.
4147,0.2412
HEATFLUX(1,3)=0.4036,0.7975,1.4569,2.0453,1.4217,0.3666,1.4217,2.0453,1.4569,0.
7975,0.4036
HEATFLUX(1,4)=0.6254,1.4405,3.3063,6.6755,8.4434,7.0409,8.4434,6.5755,3.3063,1.
4405,0.6254
HEATFLUX(1,5)=0.8428,2.1929,6.1219,16.9746,37.8951,51.4965,37.8951,16.9746,6.1
219,2.1929,0.8428
HEATFLUX(1,6)=0.9373,2.5538,7.6937,23.9587,62.1941,92.0633,62.1941,23.9587,7.6
937,2.5538,0.9373
HEATFLUX(1,7)=0.8428,2.1929,6.1219,16.9746,37.8951,51.4965,37.8951,16.9746,6.1
219,2.1929,0.8428
HEATFLUX(1,8)=0.6254,1.4405,3.3063,6.6755,8.4434,7.0409,8.4434,6.5755,3.3063,1.
4405,0.6254

```

HEATFLUX(1,9)=0.4036,0.7975,1.4569,2.0453,1.4217,0.3666,1.4217,2.0453,1.4569,0.7975,0.4036
 HEATFLUX(1,10)=0.2412,0.4147,0.6414,0.7834,0.6422,0.4630,0.6422,0.7834,0.6414,0.4147,0.2412
 HEATFLUX(1,11)=0.1404,0.2171,0.3054,0.3681,0.3726,0.3579,0.3726,0.3681,0.3054,0.2171,0.1404

/PREP7

K,7,101.6,47.625,0,
 K,8,101.6,47.625,-5.1562,
 K,9,101.6,50.8,-5.1562,
 K,10,101.6,50.8,0,
 K,11,101.6,73.025,0,
 K,12,101.6,73.025,-5.1562,
 K,13,101.6,76.2,-5.1562,
 K,14,101.6,76.2,0,
 K, 24, 0.000000, 76.20000, 0.000000,
 K,25, 0.000000, 76.20000, -5.156200,
 K,26, 0.000000, 73.02500, -5.156200,
 K,27, 0.000000, 73.02500, 0.000000,
 K, 28, 0.000000, 50.80000, 0.000000,
 K,29, 0.000000, 50.80000, -5.156200,
 K,30, 0.000000, 47.62500, -5.156200,
 K,31, 0.000000, 47.62500, 0.000000,
 K, 37, 50.80000, 47.625, -9.017000,
 K, 38, 50.80000, 47.625, -21.71700,
 K, 39, 50.80000, 76.2, -21.71700,
 K,40,50.8,76.2,-9.017,
 K,41,50.8,47.625,-15.367,
 K,42,50.8,76.2,-15.367,
 K,43,57.15,47.625,-15.367,
 K,44,44.45,47.625,-15.367,
 K,45,57.15,76.2,-15.367,
 K,46,44.45,76.2,-15.367,
 K,19,101.6,47.625,-30.734,
 K,18,101.6,76.2,-30.734,
 K,20,0,76.2,-30.734,
 K,36,0,47.625,-30.734,

LSTR, 20, 18
 LSTR, 18, 19
 LSTR, 19, 8

LSTR, 20, 36
 LSTR, 36, 30
 LSTR, 24, 25
 LSTR, 25, 26
 LSTR, 26, 27
 LSTR, 25, 13
 LSTR, 26, 12
 LSTR, 24, 14
 LSTR, 27, 11
 LSTR, 14, 13
 LSTR, 13, 12
 LSTR, 12, 11
 LSTR, 11, 12
 LSTR, 27, 28
 LSTR, 29, 28
 LSTR, 29, 30
 LSTR, 30, 31
 LSTR, 10, 9
 LSTR, 9, 8
 LSTR, 8, 7
 LSTR, 10, 9
 LSTR, 10, 11
 LSTR, 29, 9
 LSTR, 30, 8
 LSTR, 28, 10
 LSTR, 31, 7

LARC,40,46,42,6.35,
 !*
 LARC,46,39,42,6.35,
 !*
 LARC,39,45,42,6.35,
 !*
 LARC,45,40,42,6.35,
 LARC,44,37,41,6.35,
 !*
 LARC,37,43,41,6.35,
 !*
 LARC,38,43,41,6.35,
 !*
 LARC,38,44,41,6.35,

LSTR, 46, 44
 LSTR, 40, 37
 LSTR, 39, 38

LSTR, 45, 43

! /COM,Preferences for GUI filtering have been set to display:

! /COM, Thermal

!*

LSTR, 25, 20

LSTR, 13, 18

LSTR, 36, 19

FLST,2,4,4

FITEM,2,4

FITEM,2,1

FITEM,2,2

FITEM,2,42

AL,P51X

FLST,2,8,4

FITEM,2,40

FITEM,2,4

FITEM,2,5

FITEM,2,18

FITEM,2,17

FITEM,2,16

FITEM,2,8

FITEM,2,7

AL,P51X

! /VIEW,1,1,2,3

! /ANG,1

! /REP,FAST

FLST,2,8,4

FITEM,2,41

FITEM,2,14

FITEM,2,15

FITEM,2,23

FITEM,2,20

FITEM,2,21

FITEM,2,3

FITEM,2,2

AL,P51X

FLST,2,4,4

FITEM,2,11

FITEM,2,6

FITEM,2,9

FITEM,2,13

AL,P51X

! LPLOT

```
! /DIST,1,0.729,1
! /REP,FAST
! /DIST,1,1.37174211248,1
! /REP,FAST
! /ANG,1,30,XS,1
! /REP,FAST
! /VIEW,1,1,2,3
! /ANG,1
! /REP,FAST
FLST,2,4,4
FITEM,2,10
FITEM,2,9
FITEM,2,7
FITEM,2,14
AL,P51X
! /DIST,1,0.729,1
! /REP,FAST
! /DIST,1,1.37174211248,1
! /REP,FAST
FLST,2,4,4
FITEM,2,10
FITEM,2,8
FITEM,2,12
FITEM,2,15
AL,P51X
! APLOT
! /VIEW,1,-1
! /ANG,1
! /REP,FAST
! /VIEW,1,1,2,3
! /ANG,1
! /REP,FAST
ADELE, 2
! LPLOT
! /VIEW,1,1
! /ANG,1
! /REP,FAST
! /VIEW,1,-1
! /ANG,1
! /REP,FAST
! /VIEW,1,,1
! /ANG,1
! /REP,FAST
! /VIEW,1,1,2,3
! /ANG,1
! /REP,FAST
```

FLST,2,8,4
FITEM,2,16
FITEM,2,8
FITEM,2,7
FITEM,2,40
FITEM,2,4
FITEM,2,5
FITEM,2,18
FITEM,2,17
AL,P51X
FLST,2,4,4
FITEM,2,5
FITEM,2,42
FITEM,2,3
FITEM,2,25
AL,P51X
! APLOT
FLST,2,4,4
FITEM,2,25
FITEM,2,19
FITEM,2,22
FITEM,2,27
AL,P51X
! LPLOT
FLST,2,4,4
FITEM,2,26
FITEM,2,16
FITEM,2,23
FITEM,2,12
AL,P51X
! LPLOT
FLST,2,4,4
FITEM,2,29
FITEM,2,38
FITEM,2,36
FITEM,2,35
AL,P51X
FLST,2,4,4
FITEM,2,30
FITEM,2,38
FITEM,2,34
FITEM,2,39
AL,P51X
FLST,2,4,4
FITEM,2,33
FITEM,2,37

FITEM,2,39
FITEM,2,31
AL,P51X
FLST,2,4,4
FITEM,2,36
FITEM,2,37
FITEM,2,28
FITEM,2,32
AL,P51X
! A PLOT
FLST,2,4,4
FITEM,2,40
FITEM,2,1
FITEM,2,9
FITEM,2,41
AL,P51X
! SAVE, singleblock100-5,db,
! A PLOT
FLST,2,4,4
FITEM,2,29
FITEM,2,30
FITEM,2,31
FITEM,2,28
AL,P51X
ASBA, 14, 15

FLST,2,4,4
FITEM,2,18
FITEM,2,24
FITEM,2,25
FITEM,2,21
AL,P51X
! A PLOT

! L PLOT
FLST,2,4,4
FITEM,2,35
FITEM,2,34
FITEM,2,33
FITEM,2,32
AL,P51X

! A PLOT
FLST,2,4,4
FITEM,2,17
FITEM,2,26

FITEM,2,20
 FITEM,2,24
 AL,P51X

FLST,2,4,4
 FITEM,2,5
 FITEM,2,42
 FITEM,2,3
 FITEM,2,27
 AL,P51X

FLST,2,4,4
 FITEM,2,42
 FITEM,2,25
 FITEM,2,5
 FITEM,2,3
 AL,P51X
 ASBA, 7, 15

FLST,2,16,5,ORDE,6
 FITEM,2,1
 FITEM,2,-6
 FITEM,2,8
 FITEM,2,-14
 FITEM,2,16
 FITEM,2,-18
 VA,P51X

FLST,2,16,5,ORDE,6
 FITEM,2,1
 FITEM,2,-6
 FITEM,2,8
 FITEM,2,-14
 FITEM,2,16
 FITEM,2,-18
 VA,P51X
 ! L PLOT
 FLST,2,12,5,ORDE,7
 FITEM,2,1
 FITEM,2,-3
 FITEM,2,6
 FITEM,2,9
 FITEM,2,-13
 FITEM,2,16
 FITEM,2,-18

VA,P51X
 FLST,2,16,5,ORDE,6
 FITEM,2,1
 FITEM,2,-6
 FITEM,2,8
 FITEM,2,-14
 FITEM,2,16
 FITEM,2,-18
 VA,P51X

FLST,2,16,5,ORDE,6
 FITEM,2,1
 FITEM,2,-6
 FITEM,2,8
 FITEM,2,-14
 FITEM,2,16
 FITEM,2,-18
 VA,P51X
 ! L PLOT
 FLST,2,14,5,ORDE,6
 FITEM,2,1
 FITEM,2,-5
 FITEM,2,8
 FITEM,2,-14
 FITEM,2,16
 FITEM,2,18
 VA,P51X

FLST,2,2,5,ORDE,2
 FITEM,2,4
 FITEM,2,16
 ADELE,P51X
 ! A PLOT
 ADELE, 8
 ! A PLOT
 ! L PLOT

FLST,2,2,4,ORDE,2
 FITEM,2,11
 FITEM,2,27
 LDELE,P51X
 ! L PLOT

FLST,2,4,4,ORDE,4
 FITEM,2,6
 FITEM,2,13

```

FITEM,2,19
FITEM,2,22
LDELE,P51X
! LPLOT
! KPLOT,ALL
! APLOT
FLST,2,4,4
FITEM,2,40
FITEM,2,1
FITEM,2,41
FITEM,2,9
AL,P51X
! APLOT
ADELE, 4
! APLOT
FLST,2,4,4
FITEM,2,40
FITEM,2,1
FITEM,2,41
FITEM,2,9
AL,P51X
! APLOT
FLST,2,4,4
FITEM,2,29
FITEM,2,30
FITEM,2,31
FITEM,2,28
AL,P51X
ASBA, 4, 7

! SAVE, singleblock100-5,db,
FLST,2,14,5,ORDE,8
FITEM,2,1
FITEM,2,-3
FITEM,2,5
FITEM,2,-6
FITEM,2,8
FITEM,2,-14
FITEM,2,17
FITEM,2,-18
VA,P51X
! LPLOT
! VPLOT

! VPLOT
! APLOT

```

```

! LPLOT
! VPLOT
/PREP7
!*
ET,1,SOLID87
!*
!*
MPTEMP,,,,,,,,
MPTEMP,1,0
MPDATA,KXX,1,,0.365
MPTEMP,,,,,,,,
MPTEMP,1,0
MPDATA,C,1,,391
MPTEMP,,,,,,,,
MPTEMP,1,0
MPDATA,DENS,1,,8.9e-06
ADELE, 9
VDELE, 1
! APLOT
ADELE, 9
! APLOT
wpoff,50.8,61.9125,0
CSYS,4
K,100,,,
K,101,10,,
K,102,0,10,,
K,103,-10,0,,
K,104,-10,,
FLST,3,3,3
FITEM,3,102
FITEM,3,103
FITEM,3,104
BSPLIN, ,P51X
FLST,3,3,3
FITEM,3,102
FITEM,3,101
FITEM,3,104
BSPLIN, ,P51X
! LPLOT
! APLOT
! LPLOT
FLST,2,2,4
FITEM,2,6
FITEM,2,11
AL,P51X
! APLOT

```

FLST,2,4,4
FITEM,2,16
FITEM,2,12
FITEM,2,23
FITEM,2,25
AL,P51X

FLST,2,4,4
FITEM,2,16
FITEM,2,23
FITEM,2,12
FITEM,2,26
AL,P51X
! APLOT

FLST,2,2,5,ORDE,2
FITEM,2,4
FITEM,2,7
AOVLAP,P51X
FLST,2,15,5,ORDE,6
FITEM,2,1
FITEM,2,-6
FITEM,2,8
FITEM,2,-14
FITEM,2,17
FITEM,2,-18
VA,P51X
! VPLOT
!*
ANTYPE,0
!*
SMRT,6
SMRT,10
MSHAPE,1,3D
MSHKEY,0
!*
CM,_Y,VOLU
VSEL, , , , 1
CM,_Y1,VOLU
CHKMSH,'VOLU'
CMSEL,S,_Y
!*
VMESH,_Y1
!*
CMDELE,_Y

```

CMDELE,_Y1
CMDELE,_Y2
!*
SMRT,1
CM,_Y,VOLU
VSEL, , , 1
CM,_Y1,VOLU
CHKMSH,'VOLU'
CMSEL,S,_Y
!*
!*
VCLEAR,_Y1
VMESH,_Y1
!*
CMDELE,_Y
CMDELE,_Y1
CMDELE,_Y2
!*
FLST,2,4,5,ORDE,2
FITEM,2,10
FITEM,2,-13
/GO
!*
!*
SFA,4,1,HFLUX,%HEATFLUX%
!*

SFA,P51X,1,CONV,0.01553,25

! /STATUS,SOLU
SOLVE
! /VIEW,1,1,2,3
! /ANG,1
! /REP,FAST
FINISH
/POST1
! /EFACE,1
!*
! PLNSOL,TEMP, ,0,
WPSTYLE,,,,,,,,0

```

APPENDIX B

THE UNDULATOR PARAMETERS FOR THE APPLICATION OF THE VARIABLE HEAT FLUX

<http://www.aps.anl.gov/asd/me/mehome.html>

Reference: Insertion device power density calculations from the page of calculators of the APS ME (Mechanical Engineering) group website. Parameters are taken from the references [20] and [23].

1. Beam Current – 100mA
2. Beam Energy – 7GeV
3. Undulator Peak Magnetic Field – 0.27 T
4. Number of Periods, N – 198
5. Undulator Period Length – 1.8 cm
6. Source Distance – 34.1 m

Calculated total power and power density at various locations.

Total Power – 0.805 kW

Normal Peak Power Density – 92.0633 W/mm²

APPENDIX C

THE PARAMETERS FOR FILM COEFFICIENT CALCULATIONS

Reference: <http://www.aps.anl.gov/asd/me/mehome.html>

Film coefficient calculations from the page of 'Film coefficient and Pressure Drop Calculator' of the APS ME(Mechanical Engineering) group website. The parameters are given as under:

Channel Diameter: 0.5 in.

Fluid Flow: Ranging from 5 ft/sec to 30 ft/sec

Channel Length (Optional): Default value: 100 in.

Bulk Fluid Temperature (Optional): Default Value: 25⁰ C

Estimated Wall Temperature (Optional): Default Value: 25⁰ C

BIBLIOGRAPHY

1. Whitley, J. B., et al, "Engineering Considerations for the Tore Supra Pump Limiter," presented at the 14th Symposium on Fusion Technology, Avignon, France, September 1986.
2. Knuttsson, L., Mattson, E., and Ramberg, B. E., "Erosion Corrosion in Copper Water Tubing," British Corrosion Journal, Volume 7, PP. 206-211, (1972).
3. Combs, S. K., Milora, S. L., Foster, C. A., Haselton, H. H., Menon, M. M., and Tsai, C. C., "Compact, Inexpensive Target Design for Steady-State Heat Removal in High Heat-Flux Fusion Applications," Rev. Sci. Instrum. Volume 56, No. 8 pp. 1526-1530, (1985).
4. Brandes, E. A., Smithells Metals Reference Book, Sixth Edition, p. 14-16, (1983).
5. Cubberly, W. H., Metal Handbook, Ninth Edition, Volume 2, p. 771-776, (1979).
6. S. C. M. Metal Products, "Glidcop Grade Al-15 Dispersion Strengthened Copper," Technical Data, (1983).
7. Hatch, G. B., "Unusual Cases of Copper Corrosion," Journal of AWWA, pp. 1417-1428, (1961).
8. Mattsson, E., "Corrosion of Copper in Fresh Waters," paper from Australasian Corrosion Association Silver Jubilee Conference, Volume 2, pp. C-7-1 to C-7-17, (1980).

9. Bulow, C. L., "Choosing Copper Alloys for the Heat-Transfer Equipment," Chemical Engineering, Volume 70, pp. 130-134, (1963).
10. Campbell, H. S., "A Review: Pitting Corrosion of Copper and Its Alloys," Localized Corrosion, pp. 625-628, (1974).
11. Whitley, J. B., Blewer, R. S., Mullendore, A. W., "Laboratory Testing of High Flux Components," J. Vac. Sci. Technol., 20 (4), April 1982.
12. Troxell, J. D., "Glidcop Dispersion Strengthened Copper: Potential Applications in Fusion Power Generators," SCM Metal Products, Inc.
13. Incropera, F., and Dewitt D., "Fundamentals of heat and mass transfer," 2nd Ed., John Wiley & Sons, New York, 1985.
14. Davies, J. R., et al., Metals Handbook, Vol. 7 (Metals Park, Ohio: American Society of Metals, 1984), pp-711.
15. Glidcop is a registered trademark of OMG Americas Corp., Research Triangle Park, N. N. C., USA.
16. S. C. M. Metal Products, Inc. Technical Data Glidcop Grade Al-15 Dispersion strengthened Copper.
17. <http://www.MatWeb.com>, The Online Materials Database.
18. Dobson, R.L., Whitley, J. B., "Erosion Corrosion of copper in a high velocity water environment," Sandia National Laboratories.
19. Tahtinen, S., Pyykkonen, M., Smuk, S., Hanninen, H., Jagodzinski, Y., Tarasenko, O., " Fracture Toughness and Internal Friction of Glidcop Al-25 Alloy", Mat. Res. Soc. Sym. Proc. Vol. 540.
20. Yang, X., Lumpkin, A. H., Goeppner, G. A., Sharma, S., Rotela, E., Sheng, I.

C., Moog, E., "Status of the APS Diagnostics Undulator Beamline," Argonne National Labs.

21. <http://www.aps.anl.gov>, The ANL site for Advanced Photon Source.
22. K. J. Kim, "Angular Distribution of Undulator Power for an Arbitrary Deflection Parameter K," Nuc. Instr. and Meth. A246, pp. 67-70 (1986)
23. G. K. Shenoy, P. J. Viccaro, D. M. Mills, "Characteristics of the 7-GeV Advanced Photon Source: A Guide for Users," Argonne National Laboratory Report, ANL-88-9(1988).
24. Ali M. Khounsary and Barry Lai, "Power Distributions of the APS Bending Magnets and Insertion Devices" , Advanced Photon Source, ANL, July 1992.
25. John H. Lienhard, " A Heat Transfer Textbook", 1981.